

## RADIO CONTINUUM EMISSION AT 1.4 GHZ FROM KISS EMISSION-LINE GALAXIES

JEFFREY VAN DUYNÉ<sup>1</sup>, ELI BECKERMAN<sup>2</sup>, JOHN J. SALZER  
Astronomy Department, Wesleyan University, Middletown, CT 06459; slaz@astro.wesleyan.edu

CARYL GRONWALL  
Department of Astronomy & Astrophysics, Pennsylvania State University, University Park, PA 16802;  
caryl@astro.psu.edu

TRINH X. THUAN  
Astronomy Department, University of Virginia, Charlottesville, VA 22903; txt@starburst.astro.virginia.edu

J. J. CONDON  
National Radio Astronomy Observatory, Charlottesville, VA 22903; jcondon@nrao.edu

AND

LISA M. FRATTARE  
Space Telescope Science Institute, Baltimore, MD 21218; frattare@stsci.edu  
*Submitted 22 September 2003; Accepted 2 January 2004 – To appear in the April, 2004 AJ*

### ABSTRACT

We have searched the Faint Images of the Radio Sky at Twenty centimeters (FIRST) and the NRAO VLA Sky Survey (NVSS) 1.4 GHz radio surveys for sources that are coincident with emission-line galaxy (ELG) candidates from the KPNO International Spectroscopic Survey (KISS). A total of 207 of the 2157 KISS ELGs ( $\sim 10\%$ ) in the first two H $\alpha$ -selected survey lists were found to possess radio detections in FIRST and/or NVSS. Follow-up spectra exist for all of the radio detections, allowing us to determine the activity type (star-forming vs. AGN) for the entire sample. We explore the properties of the radio-detected KISS galaxies in order to gain a better insight into the nature of radio-emitting galaxies in the local universe ( $z < 0.1$ ). No dwarf galaxies were detected, despite the large numbers of low-luminosity galaxies present in KISS, suggesting that lower mass, lower luminosity objects do not possess strong galaxian-scale magnetic fields. Due to the selection technique used for KISS, our radio ELGs represent a quasi-volume-limited sample, which allows us to develop a clearer picture of the radio galaxy population at low redshift. Nearly 2/3rds of the KISS radio galaxies are starburst/star-forming galaxies, which is in stark contrast to the results of flux-limited radio surveys that are dominated by AGNs and elliptical galaxies (i.e., classic radio galaxies). While there are many AGNs among the KISS radio galaxies, there are no objects with large radio powers in our local volume. We derive a radio luminosity function (RLF) for the KISS ELGs that agrees very well with previous RLFs that adequately sample the lower-luminosity radio population.

*Subject headings:* galaxies: starburst — galaxies: active — galaxies:luminosity function — radio continuum

### 1. INTRODUCTION

Radio source surveys provide an unobstructed window for studying the distant universe. In the past few decades there have been many attempts to construct radio luminosity functions for both radio- and optically-selected surveys of galaxies (Condon 1984; Windhorst et al. 1985; Kron et al. 1985; Condon 1989; Condon, Cotton & Broderick 2002). Recently, studies have focused on more specific aspects of galaxian radio emission by either trying to obtain samples of radio sources that reach to sub-mJy flux levels (Benn et al. 1993; Gruppioni et al. 1999; Georgakakis et al. 1999; Richards 2000; Prandoni et al. 2001), or attempting to select radio galaxies from specialized subsamples (Brinkmann et al. 2000; Ho & Ulvestad 2001; Yun, Reddy & Condon 2001). However, the focus of most of these studies has been on higher redshifts. This comes

about naturally due to the use of flux-limited samples of objects. These samples are relevant for studying the evolution of the radio luminosity function. In the current study we take a different approach, seeking to investigate the radio emission from a quasi-volume-limited sample of galaxies. We explore the population of radio-emitting galaxies in the local universe ( $z < 0.1$ ) by selecting these galaxies from the KPNO International Spectroscopic Survey (KISS; Salzer et al. (2000, 2001)), which detects galaxies via the H $\alpha$  emission line.

Previous objective-prism galaxy surveys, such as the Markarian (Markarian 1967; Markarian, Lipovetskii, & Stepanian 1981), Tololo (Smith 1975; Smith, Aguirre & Zelman 1976), Michigan (MacAlpine, Smith & Lewis 1977; MacAlpine & Williams 1981), and Case (Pesch & Sanduleak 1983; Stephenson, Pesch & MacConnell 1992) surveys, have been major sources of objects from which

<sup>1</sup> present address: Department of Astronomy, Yale University, New Haven, CT 06520; vanduyne@astro.yale.edu

<sup>2</sup> present address: Harvard Smithsonian Center for Astrophysics, 60 Garden Street, Cambridge, MA 02138; eli@head-cfa.harvard.edu

we have learned much of what we know about Seyfert galaxies, starburst galaxies and even QSOs. These active galactic nuclei (AGNs) and galaxian starbursts are among the most energetic phenomena known. Quasars, by definition, are associated with intense radio emission. However, the fraction of the other types of active galaxies that have associated radio emission remains uncertain. Also in question is the fraction of less energetic or “normal” galaxies that have detectable radio emission. These galaxies may be the population that the very deep radio flux (i.e., sub-mJy level) surveys detect. Some observations in this regime (Grupponi et al. 1999; Prandoni et al. 2001) suggest that the faint radio galaxy population consists of far more “normal,” low radio power galaxies, which are more often starburst or star-forming galaxies rather than AGNs. This is in direct contrast to mJy-level surveys that are dominated by radio-loud galaxies. If this is so, these “normal” radio galaxies most likely exist in the local universe, and would make up a substantial fraction of a volume-limited radio sample.

Recent studies (Prandoni et al. 2001; Yun, Reddy & Condon 2001; Sadler et al. 2002) have used large-area optical and infrared surveys (ESO Imaging Survey, IRAS, 2dF Galaxy Redshift survey) to identify galaxies with radio sources and construct radio-galaxy samples. We utilize KISS as the selection mechanism for a local sample of radio emission galaxies which are positionally matched with radio sources identified by the combined catalogs of the Faint Images of the Radio Sky at Twenty-centimeters (FIRST) survey (Becker et al. 1995) and the NRAO VLA Sky Survey (NVSS) (Condon et al. 1998) at 1.4 GHz. The objective-prism survey method of KISS automatically assigns redshift estimates to the identified radio galaxies, and follow-up spectroscopy of these galaxies supplies the survey with activity types. Lack of follow-up spectroscopy and redshifts is the single largest obstacle to interpreting the contents of most deep radio surveys. Highly successful studies, such as the Marano Field study conducted by Grupponi et al. (1999), were conducted with only 45% of the sub-mJy sample of galaxies having spectroscopic information. More recent studies like Prandoni et al. (2001) have achieved almost 100% follow-up spectroscopy for their galaxies.

The combination of the good depth and very specific wavelength coverage of the KISS objective-prism spectra, combined with the moderately deep brightness limits of FIRST ( $S_{lim} = 1$  mJy/beam) and NVSS ( $S_{lim} \approx 2.5$  mJy/beam) gives us a unique sample of local radio-emitting galaxies that has a high degree of completeness. Furthermore, we sample intermediate and lower radio powers better than most previous studies. This is an alternative method to probing into the nature of the so-called sub-mJy population which other groups (Georgakakis et al. 1999; Prandoni et al. 2001) believe is dominated by star-forming galaxies (which KISS is sensitive to), as opposed to the radio-loud objects found typically in galaxies with early-type morphologies.

This paper is organized as follows. In §2 we briefly summarize the surveys used in the creation of this sample (KISS, FIRST, NVSS), while in §3 we discuss the optical-radio identification method, present a comparison between the FIRST and NVSS flux densities, and define the com-

plete radio-KISS sample. The radio-KISS sample properties are described in §4 as well as the properties of KISS ELGs *not* identified with radio sources. Section 5 presents the local 1.4 GHz radio luminosity function derived from the radio-KISS sample and §6 presents our conclusions.

## 2. THE GALAXY SAMPLE

### 2.1. KPNO International Spectroscopic Survey - KISS

KISS is an H $\alpha$  emission-line-selected objective-prism survey for extragalactic objects (Salzer et al. 2000). It is the first fully digital objective-prism survey for emission-line galaxies (ELGs), with all survey data acquired using the 0.61 m Burrell Schmidt telescope located on Kitt Peak. The current study makes use of the first two survey strips. The first, described in Salzer et al. (2001), coincides with the Century Redshift Survey (Geller et al. 1997; Wegner et al. 2001), covering the region RA = 12h 15m to 17h 0m, Dec = 29 - 30°, while the second strip, described in Gronwall et al. (2004a), cuts through the Boötes void (RA = 11h 55m to 16h 15m, Dec = 42.7 - 44.3°). The first survey strip was obtained using a 2048  $\times$  2048 pixel STIS CCD (S2KA) which has 21  $\mu$ m pixels with an overall field of view of 69  $\times$  69 arcmin. Each image covered 1.32 deg<sup>2</sup>. The second survey strip was taken with a SiTe 2048  $\times$  4096 CCD with a coverage area of 50  $\times$  100 arcmin (giving an area of 1.39 deg<sup>2</sup>). The pixel size of the new CCD is smaller (15  $\mu$ m), so the area covered by each image is nearly equivalent to the original STIS CCD.

The H $\alpha$ -selected (hereafter referred to as “red”) portion of the KISS objective-prism spectral data covers a spectral range of 6400 - 7200 Å. The red survey spectral data were obtained with a 4° prism, which provided a reciprocal dispersion of 24 Å pixel<sup>-1</sup> at H $\alpha$  ( $\lambda_o = 6563$  Å) for the survey strip at Dec = 30°, and 17 Å pixel<sup>-1</sup> for the 43° strip. The spectral range was chosen to have a blue limit just below the rest wavelength of H $\alpha$  and to extend up to the beginning of a strong atmospheric OH molecular band near 7200 Å. H $\alpha$  is detectable in this range up to a redshift of approximately 0.095 (Salzer et al. 2001). Along with the objective-prism images, direct images (images with no prism in front of the telescope) for each field are obtained. Images were taken through two filters ( $B$  and  $V$ ) to a depth of  $B = 21 - 22$ , which is 1 to 2 magnitudes fainter than the limiting magnitude of the spectral images. From these images, accurate positions and  $B$  and  $V$  photometry for all objects are obtained.

The ELG candidates selected by KISS are cataloged, but these remain only candidates until follow-up spectroscopy can be done for these objects. Higher resolution slit or fiber spectra have been obtained and reduced for approximately 83% of the 30 degree strip, and 30% of the newer 43 degree strip. These spectra cover a wide range of optical wavelengths, which allow for the measurement of various emission lines such as H $\alpha$ , H $\beta$ , [O III]  $\lambda\lambda$  4959, 5007 Å, [N II]  $\lambda\lambda$  6548, 6583 Å, etc. From these spectra, the activity type of the ELGs can be determined (Seyfert 1 and 2s, starbursts, Low Ionization Nuclear Emission Regions (LINERs), QSOs) as well as the metallicities of these galaxies (Melbourne & Salzer 2002).

### 2.2. Faint Images of the Radio Sky at Twenty-centimeters - FIRST

The FIRST survey is being conducted with the Very Large Array (VLA) in the B configuration at 1.4 GHz. The stated sensitivity of the FIRST source catalog is 1.0 mJy/beam, with a typical rms noise level of 0.15 mJy/beam, and an angular resolution of 5.4 arcsec FWHM (Becker et al. 1995). The sensitivity and resolution were selected to make FIRST comparable to the Palomar Observatory Sky Survey (POSS) in depth and resolution at radio frequencies, and is the highest resolution large-area radio survey available. FIRST detects an average source density of 89.5 sources per deg<sup>2</sup>. A map is produced for each field and sources are detected by using an elliptical Gaussian-fitting procedure (White et al. 1997). The catalog produced from this survey was estimated to be 95% complete at 2 mJy/beam and 80% complete at 1 mJy/beam (Becker et al. 1995).

Not only did FIRST fully overlap the area of the sky observed by KISS, but its scientific priorities complemented KISS and this radio-optical matching project. Using the B configuration of the VLA, FIRST was able to achieve positional accuracies of better than 1", which is sufficient to obtain a large number of optical identifications with low chance coincidence rates (Becker et al. 1995). For an object with an optical *V* magnitude of 20, the FIRST data have an identification error rate of 1%, while surveys taken in the C and D configurations have error rates of ~6% and ~25%, respectively (Becker et al. 1995), when dealing with radio point sources. However, the small size of the beam (5.4 arcsec) can also break up a single extended radio source into multiple FIRST sources. Thus, it is possible for an unassociated radio lobe to appear to be matched with a nearby KISS galaxy, while the actual central source of the radio emission is at a larger offset on the sky. Our method of checking for this situation is explained in Section 3.1. Another significant effect of the small beam size is that FIRST is not sensitive to extended, low-surface-brightness emission when compared to surveys with larger beam sizes, such as NVSS.

FIRST is sufficiently sensitive to detect the star-forming galaxies that have been proposed to start dominating the radio population within the flux regime of  $\leq 1$  mJy (Georgakakis et al. 1999; Prandoni et al. 2001). This correlates well with KISS which is sensitive to starburst galaxies over a large volume. Becker et al. (1995) state that at the FIRST threshold, ~75% of detected galaxies will be AGNs and the remainder are star-forming galaxies. While this may be true for the full FIRST database, we find a very different mix of AGNs and star-forming galaxies among the radio-detected KISS galaxies (see Section 3.4).

### 2.3. NRAO VLA Sky Survey - NVSS

The NVSS is a VLA radio survey that made 1.4 GHz continuum total intensity and linear polarization images utilizing the compact D configuration (Condon et al. 1998). The survey was sensitive down to 2.5 mJy/beam with rms brightness fluctuations of  $\sigma \approx 0.45$  mJy/beam and an angular resolution of 45 arcsec. The survey covers 82% of the celestial sphere, including the KISS area. While NVSS does not probe as deep as FIRST for point sources, the increased beam size allows NVSS to detect low-surface brightness extended radio sources, some of which are not detected by FIRST.

NVSS takes a different approach to compiling a radio survey than does FIRST. The most fundamental requirement in their survey is completeness. FIRST will detect fainter radio objects, but NVSS's goal is to detect all local radio emitting galaxies with uniformly accurate flux densities. The large beam size does not break up extended radio sources into multiple sources as FIRST does, so NVSS tends to be more accurate in its flux measurements of extended sources. However, NVSS is not as sensitive at detecting faint point sources, which FIRST is designed to detect.

As Condon et al. (1998) state, no single survey can combine the positive attributes of both a low resolution survey (for low-brightness sources and accurate flux densities of extended sources) and a high resolution one (for accurate radio positions and radio-source identifications with faint galaxies). Our solution to this problem is to combine the results of the radio-optical matching of FIRST and NVSS radio sources with the KISS sample. FIRST provides us with high positional accuracy of the radio sources, as well as faint point source radio detections. Alternatively, NVSS provides us with very accurate flux measurements as well as sensitivity to faint diffuse radio emission. The KISS project can then determine the activity type classification as well as other spectroscopic information, such as metal abundances and redshifts, by obtaining follow-up spectroscopy of the optical counterparts.

## 3. RADIO-OPTICAL MATCHING AND SAMPLE

The radio-optical matching procedures for FIRST-KISS and NVSS-KISS differ significantly due to the differing approaches, resolutions, and parameters used by the FIRST and NVSS surveying teams. Both procedures utilize the KISS direct images and the Digitized Sky Survey (DSS) optical images as the comparison to the FIRST and NVSS radio emission.

### 3.1. FIRST-KISS

Both the FIRST survey and KISS have relatively high angular resolutions (5.4 arcsec for FIRST, 3–4 arcsec for KISS), which provides accurate sky positions for the objects contained in both surveys. Because of this high level positional accuracy, we chose to perform a direct positional comparison between the surveys. We overlaid the KISS direct image of each survey field with the positions of the FIRST sources covering the KISS field of view. Figure 1 displays the results of a positional matching exercise for a random sampling of ten KISS fields and includes all the FIRST object matches to any KISS ELG with positional offsets of under 60 arcseconds. The linear increase of matches at large  $\Delta R$  is indicative of the increase of spurious matches at larger and larger radii (since the areas of the annuli around each target galaxy increase linearly with  $\Delta R$ ). A linear fit through the origin out to 60 arcseconds divides the sample into the real and spurious matches. The lower histogram shows the difference between the full set of matches and the linear fit. The fraction of spurious matches is very low for separations under 2 arcseconds (~1%). Based on these results, we decided to accept any radio source match that has a  $\Delta R < 2.0$  arcsec as a valid match as long as the radio source was unresolved (i.e., a point source). Following this decision we visually exam-

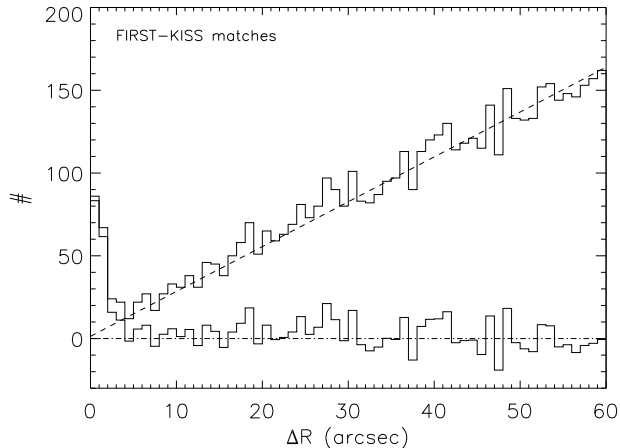


FIG. 1.— FIRST-KISS positional offsets of 10 randomly selected fields for all objects matched out to 60 arcsec separations. The dashed line represents a linear fit with an intercept constrained to zero. The lower histogram is the difference between actual matches and the linear fit at each bin. Matches with  $\Delta R$  of less than 2 arcseconds have a low proportion of spurious detections.

ined the remaining putative matches. Due to the angular size of these sources, we assume that real point source matches are only possible with offsets under 10 arcsec. True matches of point radio sources to optical galaxies should be close to the central region of the galaxy. True radio source matches at greater offsets should only be extended sources, i.e. lobe sources from an AGN or extended radio emission from a starburst region of large angular size. The remaining radio source matches with  $\Delta R > 2$  arcsec required visual verification (see below) but very few were accepted as *bonafide* matches. We did not attempt to match radio sources at  $\Delta R > 30$  arcsec due to the high resolution and precision of KISS and FIRST source positions and the increasing number density of point sources at these radii, which will only contribute spurious sources to our radio-optical sample.

When carrying out our matching procedure, we were careful not to exclude possible matches of radio sources with extended lobe morphologies with optical counterparts at larger  $\Delta R$ . Thus, we chose any KISS object within 30 arcsec of an *extended* FIRST source to be a potential match to that source. The radio positions and morphologies of these sources were visually checked by utilizing the FIRST survey field cutout web tool (<http://sundog.stsci.edu/>), which we used extensively to reduce the identification error rate even further. By utilizing the KISS object position, we can determine if the radio source is sufficiently centered in the FIRST radio field image. This is enough for verifying point sources with  $\Delta R > 2.0$  arcsec, but the radio field image also allows us to determine if an extended source is a radio lobe that has its emission source centered on the KISS object. In the end, no such lobe sources were accepted as positive matches.

Out of a possible 2157 KISS ELGs, 184 FIRST radio matches were verified. Figure 2a shows the distribution of positional offsets for the matched ELGs. The few matches beyond 2 arcsec were visually verified. The median value of the offsets (0.75 arcsec) further strengthens our confidence that  $\sim 99\%$  of the matches within 2 arcsec are real matches.

### 3.2. NVSS-KISS

The 45 arcsec angular resolution of NVSS requires a different approach to the positional matching of the KISS galaxies. Using Digitized Sky Survey (DSS) images of the KISS field of view, we overlaid NVSS radio contours to aid our search for true positional matches. Finder fields of every KISS object with an NVSS radio source within 60 arcsec were generated. Using the intensity contour lines as guides, we found that the majority of NVSS matches were visually centered on the optical KISS object. However, their positional offsets were typically much higher than the FIRST offsets shown in Figure 2a. Those radio contours that were not directly centered on an object were examined to a fainter contour level for a KISS object, unless the morphology suggested a more complex lobe structure. Furthermore, for any source match that we could not decide upon by eye, we input the radio position into the FIRST radio field cutout tool. The FIRST images usually had at least some radio emission above the noise ( $2 - 3\sigma$ ), sufficient to decide if the radio source was indeed associated with the matched KISS object.

The NVSS-KISS comparison found 23 matches that the FIRST-KISS comparison did not, all of them extended radio sources. In addition, there are 124 NVSS-KISS matches that were also found by the FIRST-KISS comparison. An additional 60 sources were detected only by FIRST. By performing the FIRST matches prior to the NVSS matches, we knew which objects were matched to FIRST radio sources. We then have more confidence in our verification of complex or weak NVSS contour lines around a KISS object. Figure 2b displays  $\Delta R$  for all NVSS matched sources. A high fraction of matches (82%) are found within 8 arcsec, and the median  $\Delta R$  is 3.45 arcsec. This low median value increased our confidence in our positional accuracy. In total, 207 KISS ELGs were matched to radio sources.

### 3.3. Radio-flux adjustments

#### 3.3.1. Improving flux measurements

FIRST uses a two-dimensional Gaussian profile to measure the flux of all FIRST radio sources. This method is

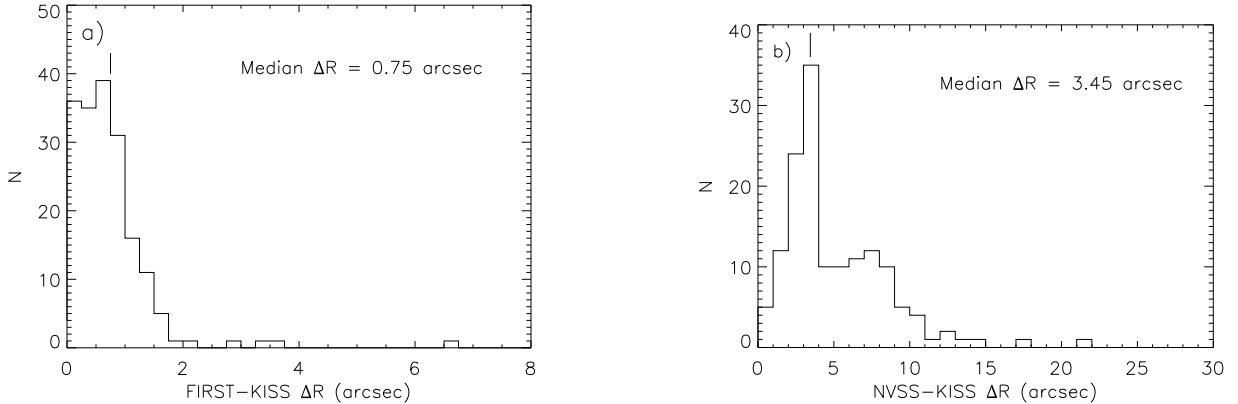


FIG. 2.— Distribution of the (a) FIRST-KISS and (b) NVSS-KISS positional offsets of verified source matches.

accurate for point sources, but the use of this fixed function will underestimate the flux of extended FIRST sources, especially radio lobe sources. To rectify this problem, we downloaded the public domain FIRST FITS files from the FIRST website for all apparently extended FIRST sources, and measured their total (integrated) radio fluxes using the IRAF PHOT task. Using the IRAF photometry of 28 point source radio galaxies with FIRST integrated fluxes ranging from 0.8 mJy to 402.0 mJy as calibration sources, we derived the following relationship:

$$F_{IRAF} = (10.185 \pm 0.002)F_{int} \quad (1)$$

where  $F_{IRAF}$  is the flux measured by IRAF in counts, and  $F_{int}$  is the integrated FIRST flux in mJy. This relationship was used together with our IRAF-based measurements of the total radio fluxes to arrive at revised estimates of  $F_{int}$  for the extended FIRST objects. Of the 19 candidates for re-measurement, 9 had at least a 10% increase in flux, with one object having a flux increase from 3.62 mJy to 242.3 mJy after including flux from associated radio lobes. Only those measurements with an increase of at least 10% had their fluxes adjusted. Table 1 contains the original and re-measured flux values.

### 3.3.2. Comparison of FIRST and NVSS flux scales

In order to combine the matching results from the FIRST and NVSS samples, we had to determine the relationship between the flux scales of the two surveys. We compiled a list of all 124 KISS ELG matches that had detections by both FIRST and NVSS. We plot the NVSS flux *versus* FIRST flux in Figure 3, as well as the NVSS/FIRST flux ratio *versus* the FIRST flux in Figure 4. The flux ratio plot shows a large discrepancy between measurements of radio sources with FIRST fluxes less than 5 mJy. This is not unexpected, as extended, low flux galaxies detected in both surveys will be resolved out by FIRST. In order to quantify the differences between the FIRST and NVSS fluxes, we performed a number of statistical comparisons. In doing so, we constrain the calculations to radio sources with the flux range of  $5 \leq F_{FIRST} \leq 60$  mJy. This is because at lower fluxes we get much larger discrepancies in flux primarily due to the difference in beam size of the two surveys. At fluxes within our chosen range, which are more likely point sources, the scaling is far more consistent. The upper limit was chosen to avoid small-number

statistical effects and because the high flux objects tend to show extreme discrepancies between FIRST and NVSS.

The line shown in Figure 3 is determined by a linear least squares fit to the galaxies in the flux density range defined above. The fit yields the equation:

$$F_{NVSS} = (1.110 \pm 0.024)F_{FIRST} - (0.152 \pm 0.394). \quad (2)$$

The mean value of the NVSS/FIRST flux ratio using the same galaxies is found to be  $\mu_{ratio} = 1.099 \pm 0.028$ , with a median of 1.061 and a standard deviation of  $\sigma = 0.194$ . The slope of the linear fit and the mean ratio value agree to within the errors, as they should.

For consistency throughout the radio-KISS sample, we chose to adjust the NVSS fluxes to the FIRST fluxes by dividing all NVSS-only detected radio sources by 1.10. Any galaxy that was matched to both FIRST and NVSS retained the FIRST flux value. This is not to imply that the NVSS fluxes are inferior to the FIRST fluxes. On the contrary, they appear to be more accurate, in the sense that they include more of the extended low surface brightness emission than does FIRST. However, since FIRST sources outnumber NVSS detections, we decided to scale the fluxes to the FIRST scale for subsequent analysis.

### 3.4. Final Sample

In Table 2, we present the number of KISS galaxies with FIRST and NVSS radio source matches, broken down by ELG type. A total of 207 KISS ELGs out of the entire KISS sample of 2157 ELG candidates were successfully matched with a radio source from either FIRST or NVSS. FIRST-KISS matched 184 galaxies while NVSS-KISS matched 147 galaxies. A total of 60 galaxies were matched only by the FIRST survey (all low flux sources) and 23 galaxies were matched only by NVSS (mostly slightly extended radio sources with lower radio surface brightness than the rest of the sample). In the cases that both surveys have sources matched to the same KISS object, the FIRST flux has been used in the analysis. All 207 radio-detected KISS galaxies possess follow-up spectra. Note that 10 galaxies are actually high redshift (i.e.  $z > 0.3$ ) objects and do not lie within the H $\alpha$  selection volume (to  $z = 0.095$ ). These ELGs were detected by KISS via their [O III]  $\lambda\lambda 4959, 5007$  Å lines, which had been redshifted into the wavelength range used by

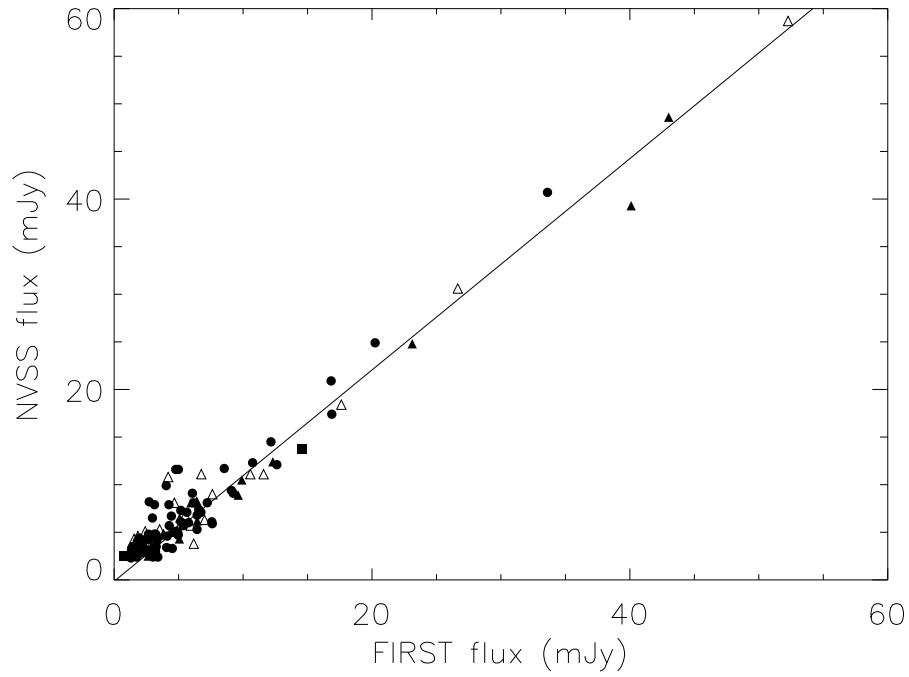


FIG. 3.— Flux density comparison between galaxies detected by both FIRST and NVSS. The least squares linear fit (see Eq.2) is used to rectify the different flux scales. Symbols represent different ELG types: Seyfert 1s (squares), Seyfert 2s (filled triangle), starbursts (circles), and LINERs (open triangle).

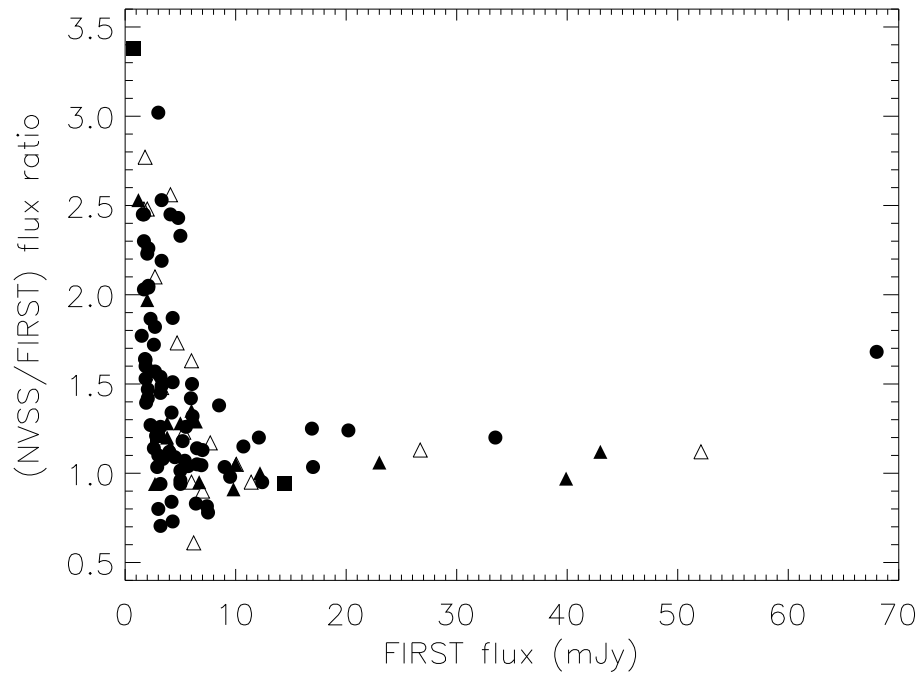


FIG. 4.— The ratio of the NVSS to FIRST radio fluxes vs. the FIRST survey flux for the same galaxies plotted in Figure 3. The mean ratio for sources with  $F_{FIRST}$  between 5 and 60 mJy is 1.10.

KISS. One exception is the QSO KISSR 844, which is at a redshift of  $z=0.46$  and was detected by  $H\beta$ . In order of contribution to the radio sample, the activity types of the radio-detected ELGs are: starburst/star-forming galaxies (63.8%), LINERs (17.9%), Seyfert 2s (15.5%), Seyfert 1s (2.4%), and QSOs (0.5%). The AGNs (LINERs, Seyferts, and QSOs) contribute a total of 36.2% of the radio-detected KISS galaxies, which is substantially higher than the 14.7% AGN fraction in the overall KISS sample among those objects with existing follow-up spectra.

While only a relatively small fraction of the KISS star-forming galaxies have radio detections (132 of 960, or 14%), roughly half of Seyfert 2s and LINERs in the KISS sample that have been identified via follow-up spectroscopy have also been detected as radio sources. Of the 64 Seyfert 2 galaxies identified by KISS, 32 (50%) are detected radio sources. Similarly, of the 76 identified LINERs, 37 (49%) have radio emission. The large number of LINERs in relation to the overall sample of radio emitting ELGs is unusual and surprising. Previous deep radio surveys have typically found only very few LINERs. Furthermore, previous optical objective-prism surveys, traditionally carried out in the blue portion of the spectrum, have missed most galaxies we would classify as LINERs. The combination of the  $H\alpha$ -selection method used by KISS and the excellent sensitivity of the two radio surveys is presumably the reason for the high number of LINERs present in the current sample. Somewhat surprisingly, only 5 of the 20 identified Seyfert 1s (25%) have associated radio emission. Note that the numbers above include the high redshift objects. If these are excluded the disparity between the two Seyfert classes becomes even worse. For the Seyferts with  $z < 0.08$ , 2 of 11 Seyfert 1s (18%) are radio detected, as opposed to 21 of 35 Seyfert 2s (60%).

A *naive* interpretation of the unified model for AGN (e.g., Schmidt *et al.* 2001; Meier 2002; Veilleux 2003) would suggest that Seyfert 1s and 2s would be detected at a similar rate in the radio continuum, unless beaming effects are important, in which case the Seyfert 1s would be expected to be stronger. Yet the Seyfert 2s greatly outnumber the broad-lined Seyferts in terms of radio detections. The apparent disparity between the fraction of radio detections in the two types of Seyferts might be explained if some or all of the radio emission detected in the Seyfert 2s were due to circumnuclear star-formation activity rather than being associated with the AGN. A test of this hypothesis could be achieved by evaluating the spatial distribution of the radio emission: extended radio emission would indicate a star-forming origin, while a radio point source would be consistent with pure AGN emission. Evaluation of the radio maps obtained by FIRST indicate that all of the KISS Seyfert galaxies detected in the radio are in fact point sources. None show extended emission. However, given the typical distance of the KISS Seyferts and the spatial resolution of the FIRST data, this is not a sensitive test. For example, the 5.4 arcsec FWHM for a FIRST point source corresponds to a linear size of 7.3 kpc for a galaxy with  $z = 0.07$ . In nearly all cases, any putative circumnuclear star-forming region would not be resolved from the central AGN in the FIRST radio maps. Hence, we cannot resolve the question of whether star-formation

activity is enhancing the radio emission from some of the Seyfert 2s. It should also be noted that there is no obvious reason why circumnuclear star-formation should preferentially be favored in the Seyfert 2s over the Seyfert 1s; the unified model does not predict any such difference. Clearly, further work in this area will be necessary.

It is worth noting that the percentages quoted in the preceding paragraph refer to the fraction of KISS ELGs that currently have follow-up spectra. While 100% of the radio-detected objects have follow-up spectra (i.e., they were targeted for observation), only 58% of the entire sample of 2157 KISS ELGs from the two survey strips studied have been observed spectroscopically. Hence, the percentages of radio-detected KISS galaxies of all activity types will go down as the follow-up spectroscopy becomes more complete.

It should also be noted that since we are using an optical line-selected galaxy catalog, we do *not* detect any early-type, elliptical galaxies. This is in contrast to previous studies of radio-selected samples where early-type galaxies are the dominant radio-emitting galaxy type at this flux level (Prandoni *et al.* 2001; Georgakakis *et al.* 1999; Magliocchetti *et al.* 2000; Gruppioni *et al.* 1999). This is discussed and addressed further in §5 and §6.

Table 3 presents the primary optical and radio characteristics of all 207 radio ELGs found in this study. The columns are as follows: (1) *KISSR*, the KISS ID of the galaxy as listed in Salzer *et al.* (2001) and Gronwall *et al.* (2004a); (2) *RA* and (3) *Dec*, given for equinox J2000. These are the optical positions tabulated in the survey papers (Salzer *et al.* 2001; Gronwall *et al.* 2004a), and have precisions of  $\sim 0.25$ – $0.30$  arcsec; (4) *B*: apparent magnitude in the Harris *B* filter (Salzer *et al.* 2001; Gronwall *et al.* 2004a); (5)  $M_B$ : absolute *B* magnitude (see below); (6)  $L_{H\alpha}$ :  $H\alpha$  line luminosity in erg/s; (7)  $S_{1.4}$ : radio flux density at 1.4GHz in mJy. If the galaxy was detected in both FIRST and NVSS, the FIRST flux value is listed. If only detected by NVSS, the flux is corrected as described above; (8)  $P_{1.4}$ : radio luminosity at 1.4 GHz in W/Hz. The luminosity is calculated from the distances derived from the listed redshift value (See § 3.4.1); (9) *z*: spectroscopic redshift (corrected for Local Group motion) obtained from the follow-up spectra; (10)  $\Delta R$ : the positional offset of the optical-radio matches in arcseconds. This value is calculated from the angular distance between the peak optical emission of the KISS object and the peak radio emission; (11) Survey match: indicates which radio survey the KISS object was matched with: F for FIRST only, N for NVSS only and B for both surveys; (12) ELG type: the activity type of the ELG as determined from follow-up spectra. The ELG activity types are as follows; Sy1: Seyfert 1; Sy2: Seyfert 2; SB: starburst or star-forming galaxy; LIN: Low Ionization Nuclear Emission Region (LINER); and QSOs.

### 3.4.1. Luminosity calculations

The absolute magnitudes and luminosities in Table 3 were calculated by using the redshifts obtained through follow-up spectroscopy. The typical error for our spectroscopic redshifts is  $\pm 30$  km/s. For all distance-dependent quantities, we assume  $H_0 = 75$  km/s/Mpc and  $q_0 = 0.5$ . Distances were derived from the observed redshifts, assuming a pure Hubble flow and after correcting for the

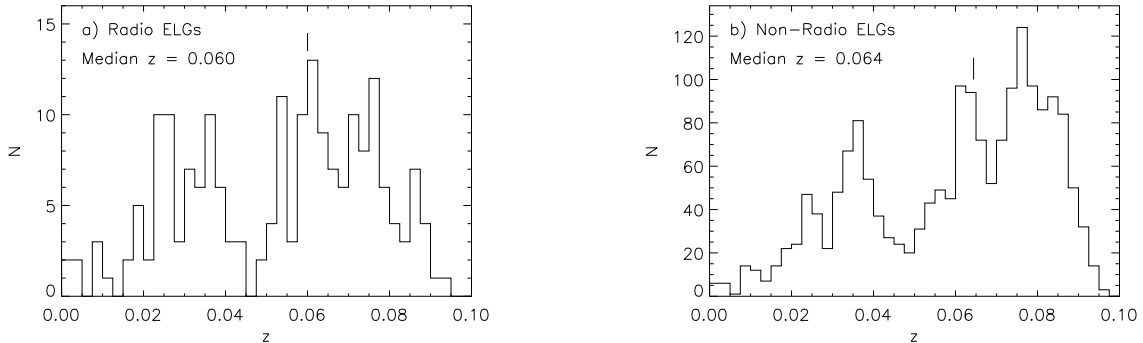


FIG. 5.— Redshift distribution of (a) radio and (b) non-radio detected ELGs in the KISS sample. The bimodal distribution is due to the low-density regions at roughly  $z = 0.045$  in both survey strips. The median redshift is essentially the same for both samples, and the two redshift distributions are statistically indistinguishable.

motion of the sun relative to the center of mass of the Local Group ( $v_{corr} = v_{helio} + 300 \sin l \cos b$ ). The  $H\alpha$  luminosities were calculated from the  $H\alpha$  flux measured from the objective-prism spectra (Salzer et al. 2001). This was done to remove slit/fiber effects which lead to the potential for loss of flux with some of our follow-up higher resolution spectroscopy. Use of the objective-prism  $H\alpha$  fluxes provides a uniform, homogeneous data set to work with, but requires us to correct for the additional flux contributed by the nearby  $[N II](\lambda\lambda 6583, 6548 \text{ \AA})$  lines that are blended with  $H\alpha$  in the objective-prism spectra. Additionally, we correct for intrinsic absorption due to dust using the Balmer decrement coefficient measured from follow-up spectra.

#### 4. RADIO PROPERTIES OF THE KISS ELGS

In this section, we present a breakdown and comparison of the optical characteristics between the radio and non-radio detected KISS ELGs, as well as the radio properties of the radio-detected sample. We also explore the metallicity and line ratio characteristics of the two samples in an effort to better understand what physical differences lie between radio and non-radio emitting ELGs.

##### 4.1. Comparison Between Radio and Non-Radio ELGs

The KISS data set provides us with a tremendous opportunity to study in detail the physical characteristics of radio-emitting galaxies that possess strong emission lines and compare them to the remainder of the KISS sample that was not radio detected. While obtaining redshifts and distances to galaxies selected in optical emission-line surveys is a trivial matter, it is much more difficult for objects discovered in radio surveys. Only through obtaining spectroscopy of the radio sources' optical counterpart can accurate distances be obtained. However, these optical counterparts are typically extremely faint, when detected at all. In the current study we resolve this problem by considering the radio characteristics of a deep sample of optically-selected ELGs (with its built-in redshift limit) rather than the optical characteristics of a radio flux-limited sample. In this case, the optical matches are all relatively bright, most with B magnitudes 18.5 or brighter.

Figure 5 shows the redshift distribution of the (a) radio and (b) non-radio ELGs. The decrease in the numbers of

galaxies at  $z \approx 0.045$  is due to the Boötes void that is present within the 43 degree strip, and a corresponding low-density region at approximately the same distance in the 30 degree strip. The redshift distribution of the non-radio-detected sources (Figure 5b) increases steadily out to  $z \approx 0.075$ , after which it falls off to zero at  $z \approx 0.095$ . This cut-off in the sensitivity of the survey is caused by the filter employed in the objective-prism observations. At redshifts above  $z \approx 0.075$ , the  $H\alpha$  line starts to redshift out of the filter bandpass (Salzer et al. 2000). Those ELGs with the strongest  $H\alpha$  emission lines are preferentially detected at the higher redshifts as the filter will cut off weaker emission. This explains the drop off at  $z > 0.075$  as a completeness effect. Below this redshift the survey is highly complete, but at higher redshifts it misses some percentage of weaker-lined ELGs. Not shown in Figure 5 are the approximately 2% of all ELGs in the KISS survey that are located at  $z > 0.3$ . These objects are detected by some line other than  $H\alpha$  in the bandpass of the objective-prism spectra (typically  $[O III]\lambda 5007$ ,  $H\beta$ , or  $H\gamma$ ).

The two redshift histograms appear to be quite similar, as are the median values of the redshift distributions ( $z = 0.060$  and  $z = 0.064$  for radio and non-radio, respectively). We might infer that the two sets of redshifts are drawn from the same parent population. Applying a KS test to the data confirms this suspicion at the 99% confidence level: the radio and non-radio ELGs exhibit the same redshift distributions.

The apparent magnitude distribution (Figure 6) shows that the radio ELGs are brighter objects (median = 16.80) than ELGs without radio emission (median = 18.22). This is a real effect, as KISS is sensitive to faint dwarf ELGs, shown by the tail of counts at  $B \geq 20$  in Figure 6b. Few galaxies with  $B > 18$  are radio detected, and those that are tend to be the high redshift objects ( $z > 0.3$ ) mentioned above. Approximately half of all ELGs brighter than  $B = 16$  are radio detected. In contrast, the typical optical counterparts to faint radio sources tend to be very faint. The reason the KISS radio sources are so bright is due to the redshift limit imposed by the survey filter combined with the fact that radio-emitting galaxies tend to be fairly luminous (see below).

A better representation of the physical characteristics of the galaxies that are being detected in the radio is found



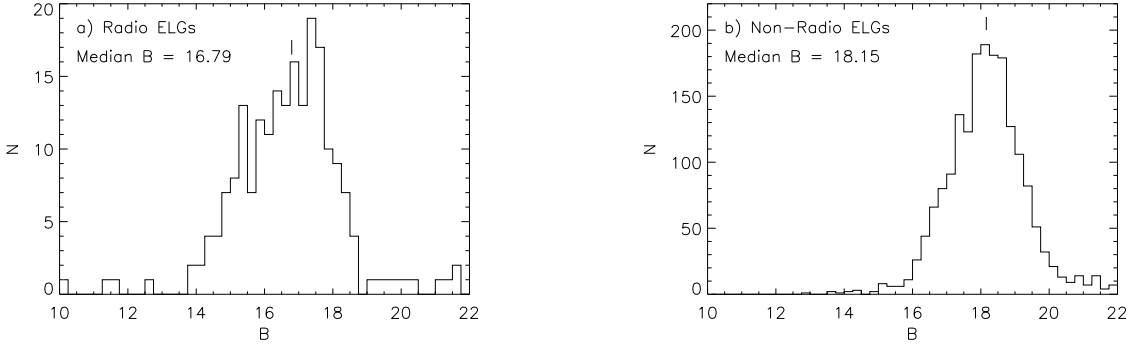


FIG. 6.— Apparent B magnitude of (a) radio and (b) non-radio detected ELGs. The radio ELGs contain the brighter portion of the overall KISS population and have a median 1.35 mag brighter than the remaining ELGs.

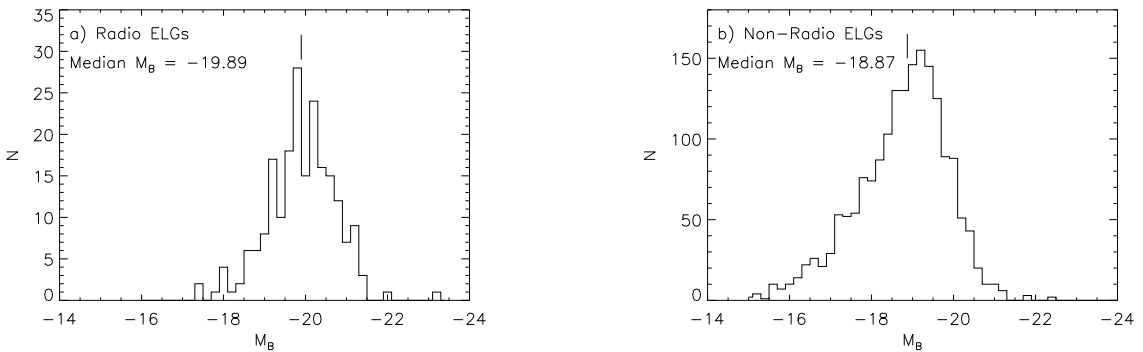


FIG. 7.— Absolute B magnitude comparisons. The radio ELG population makes up a large percentage of the optically most luminous portion of the overall KISS sample. No low luminosity galaxies (i.e. dwarf galaxies) of  $M_B > -17$  have radio detections.

in Figure 7, which plots histograms of the absolute magnitude  $M_B$ . There are two particularly interesting features of note. First, the radio population is much more luminous than the non-radio. Figure 7a shows that the radio-detected ELGs display a relatively tight distribution of absolute B magnitudes with a median value of  $-19.89$  mag. The median  $M_B$  is 1.02 mag brighter than for the non-radio KISS ELGs. The more luminous, and hence, more massive galaxies of the sample are the radio emitters (Condon 1992). However, there is a sharp cut-off at the high luminosity end. There are very few galaxies more luminous than  $M_B = -21$ , and most of these are high redshift objects ( $z > 0.3$ ). Thus, no exceptionally luminous galaxies have been radio detected within the  $H\alpha$ -selected KISS survey volume.

Second, Figure 7b shows a low-luminosity tail at  $M_B \geq -17$ , which represents the many dwarf ELGs that KISS detects within our volume. However, within the radio distribution, there are *no* galaxies fainter than  $M_B > -17$ , and only a few with  $M_B > -18$ . To emphasize the lack of galaxies with low optical luminosities within the radio-detected sample, consider that a galaxy with  $P_{1.4GHz} = 10^{21}$  W/Hz would be detectable out to a redshift of  $z = 0.023$  by FIRST. There are 130 KISS ELGs with  $z \leq 0.023$ . Of these, 42 have  $M_B$  brighter than  $-18$ , and 15 of these (35.7%) are radio detected. The remaining 88 have  $M_B$  fainter than  $-18$ , and only two are radio detected (2.3%). If the low-luminosity ELGs were detected in the same proportion as the higher-luminosity sample, there

should be 31 radio detections in the former sample. If the low-luminosity ELGs, which are all star-forming objects, were detected at the same percentage as the overall population of KISS star-forming galaxies (13.75%, see section 3.4), there would still be 12 with radio detections. A possible implication for the low proportion of dwarf galaxies within the KISS radio sample is that these low luminosity, low mass galaxies are not massive enough to produce a galactic-scale magnetic field of sufficient strength to confine the starburst’s relativistic charged particles that give rise to radio synchrotron emission. This point is discussed further in Section 4.2

A good measure of the level of star-formation within an ELG is the strength of certain emission lines, especially  $H\alpha$ . In Figures 8 and 9 we show the distribution of equivalent widths and  $H\alpha$  luminosities, respectively, for both the radio and non-radio sub-samples. The distribution of equivalent widths reveals a selection effect inherent in KISS (Salzer et al. 2000, 2001) where the survey is incomplete at low equivalent widths ( $EW < 30 \text{ \AA}$ ). This is seen in Figure 8b, where the distribution peaks at  $\sim 30 \text{ \AA}$ . Figure 8a reinforces the fact that radio emission favors high luminosity galaxies (Kellerman & Owen 1988; Figure 7), which tend to correspond to lower equivalent widths. The median equivalent width of the radio sub-sample is  $29.2 \text{ \AA}$ , compared to  $42.7 \text{ \AA}$  for the non-radio ELGs. Figure 9 shows that strong radio emission tends to be associated with high  $H\alpha$  luminosities. The median  $L_{H\alpha}$  value for the radio subset is a factor of 5 greater than the non-radio

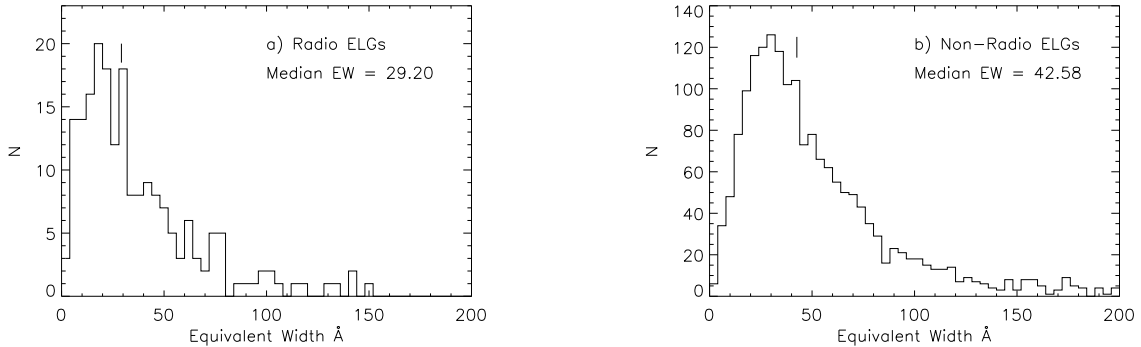


FIG. 8.— Equivalent widths of the  $H\alpha$  emission line from the objective-prism spectra for (a) radio and (b) non-radio ELGs.

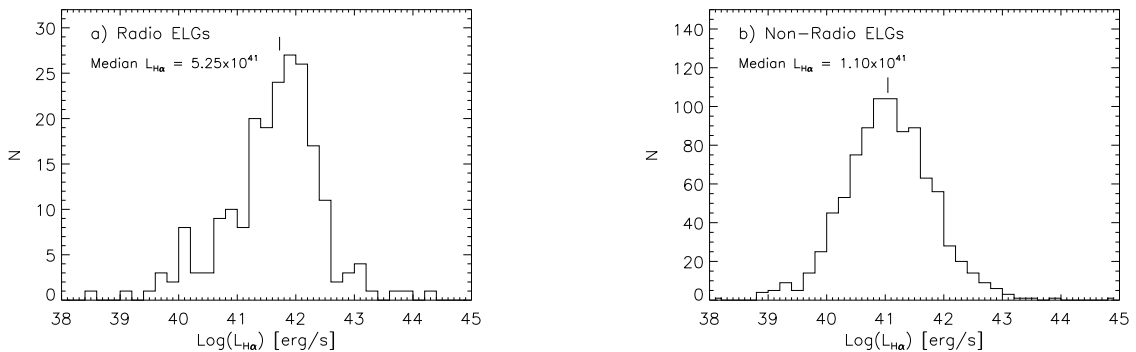


FIG. 9.— (a) Radio and (b) non-radio ELG  $H\alpha$  line luminosities.

ELGs. Discussion of the relationship between  $L_{H\alpha}$  and radio power is deferred to a future paper which presents the IRAS FIR properties of the KISS ELGs and compares star-formation rate estimates derived from FIR, radio, and  $H\alpha$  luminosities (Gronwall et al. 2004c).

#### 4.1.1. Line Diagnostic Diagrams

The follow-up spectroscopy obtained for the KISS ELGs allows us to generate diagnostic diagrams of all galaxies with spectra of sufficient quality to obtain line ratios. Figure 10 displays a diagnostic diagram for both the radio-detected and full KISS samples. Plotted is the ratio of  $[OIII]/H\beta$  vs. the ratio of  $[NII]/H\alpha$ . Different symbols denote different types of active galaxies: Seyfert 2 galaxies (filled triangles), LINERs (open triangles), and star-forming galaxies (filled circles). While star-forming galaxies typically lie along the HII sequence, AGNs have line ratios of  $\text{Log}([NII]/H\alpha) > -0.4$  and lie above and to the right of the star-forming galaxies. Seyfert 2s are located at high values of  $[OIII]/H\beta$  ( $> 3$ ), while the LINERs are located between the Seyferts and starburst galaxies (Baldwin, Phillips, & Terlevich 1981; Veilleux & Osterbrock 1987).

Figure 10b shows all the KISS ELGs with follow-up spectroscopy of sufficient quality to measure the necessary line ratios. While not all the KISS ELGs have follow-up spectra, all of the radio subset have follow-up spectra and are represented in Figure 10a. The distribution of Seyferts and LINERs in the two diagrams is very similar. This should not be a surprise, since a large fraction of the over-

all KISS AGNs are radio detected. As mentioned above, 50% of both the Seyfert 2s and LINERs identified in KISS are detected as radio sources. The radio-detected starburst galaxies are concentrated toward the high luminosity, high metallicity end of the HII sequence, while the full KISS sample populates the sequence more uniformly. As mentioned previously, starburst galaxies with detectable radio sources are generally limited to higher luminosity galaxies. These relatively high mass galaxies have high metallicities, which place them in the lower right section of the HII sequence (Melbourne & Salzer 2002). Compared to the full KISS sample, which spans the full range of metallicities observed in galaxies, the radio sample includes only a modest number of intermediate metallicity ELGs (central portion of the HII sequence) and no low abundance objects (upper left portion of the sequence).

#### 4.2. Radio Characteristics

Due to the extremely faint (in the optical) nature of many of their constituents, early radio-optical surveys (Windhorst et al. 1985; Benn et al. 1993) experienced difficulty obtaining spectroscopy for the majority of their sample. Thus, these surveys dealt primarily with the radio flux aspect of the sources. Recently, radio samples have been constructed for which follow-up spectroscopy for most, if not all, galaxies could be obtained (Prandoni et al. 2001; Sadler et al. 2002; Yun, Reddy & Condon 2001). Consequently, radio luminosities and activity types could be derived for the majority of the galaxies, providing a more complete understanding of the nature of the galaxies con-

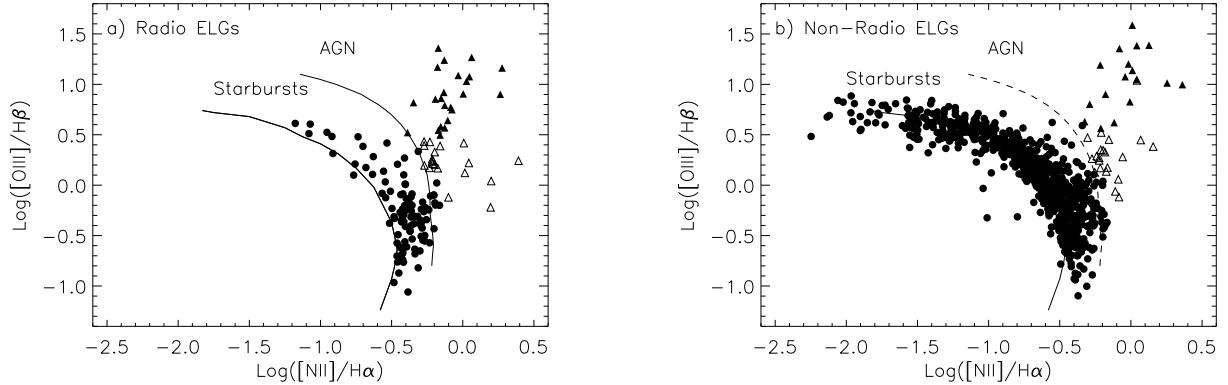


FIG. 10.— Line diagnostic diagrams of the (a) radio-detected subset (145 ELGs) and (b) entire KISS sample with high quality follow-up spectroscopy (633 ELGs). ELGs with follow-up spectroscopy of insufficient quality to measure all four emission lines ( $H\alpha$ ,  $H\beta$ ,  $[N II]$ , and  $[O III]$ ) are not displayed. Symbols represent Seyfert 2s (filled triangles), LINERs (open triangles), and starbursts (circles).

tained in the sample. All of the galaxies in the current study have redshifts and detailed spectral data available.

Figures 11 and 12 show the distribution of integrated radio fluxes and radio luminosities of all 207 radio-KISS ELGs. The majority of the sample lies in the 1 - 10 mJy flux range, similar to Kron *et al.* (1985) and Windhorst *et al.* (1985). Due to the volume limits imposed by our filter and optical selection method, we do not need to go to sub-mJy fluxes (Benn *et al.* 1993; Georgakakis *et al.* 1999; Gruppioni *et al.* 1999; Prandoni *et al.* 2001) to obtain a substantial sample of nearby, low-luminosity radio-emitting star-forming galaxies. In Figure 11, there are galaxies with integrated fluxes below 1.0 mJy. While FIRST has a stated flux limit of 1.0 mJy, the integrated flux density of FIRST sources can drop slightly below 1 mJy. Those galaxies in Figure 11 with relatively high fluxes ( $S_{1.4GHz} \geq 100$  mJy) include one very nearby LINER, NGC 4278 (KISSR 29,  $z=0.0020$ ), the nearby giant irregular NGC 4449 (KISSR 1307,  $z=0.00063$ ), and two high redshift Seyfert 2s (KISSR 1304,  $z=0.3481$  and KISSR 1561,  $z=0.3380$ ), which have radio luminosities typical of classic radio galaxies. The rarity of high flux sources in the main KISS volume ( $z < 0.095$ ) shows how uncommon it is to find extremely bright sources locally. This point will be discussed further when we present the radio luminosity function for the KISS sample in §5.

The radio power distribution (Figure 12) shows a narrow distribution, with a median value of  $P_{1.4GHz} = 1.63 \times 10^{22}$  W/Hz. There are 15 galaxies with radio powers less than  $3 \times 10^{21}$  W/Hz, which represent the low end of the radio luminosity distribution. All are classified as star-forming galaxies. At the other extreme, there are 27 galaxies with radio luminosities greater than  $5 \times 10^{22}$  W/Hz. However, 10 of these galaxies have high redshifts ( $z > 0.095$ ) and are not within the main survey volume. These are represented by the heavy histogram in Figure 12. They will not be included in any further analysis in this paper because they were not detected via the  $H\alpha$  emission line, but by redshifted  $[OIII]\lambda 5007 \text{ \AA}$  or  $H\beta$  emission lines. This high- $z$  population is composed of seven Seyfert 2s, two Seyfert 1s, and one QSO. They are good examples of the radio-loud galaxies typically found in standard flux-limited radio surveys. Excluding these high redshift galaxies, we have

a relatively well-defined upper limit to our radio luminosity distribution; only three galaxies have  $P_{1.4GHz} \geq 10^{23}$  W/Hz. Within the KISS volume, we find that there are *no* prototypical “radio galaxies” (Condon 1992) like those found in standard flux-limited surveys. In such surveys, these extremely luminous galaxies are easy to detect out to great distances, but as we show in Figure 12, they are not the most common type of radio emitting galaxy in the local universe. These radio-loud objects are analogous to O stars in stellar populations, easy to detect due to their high intrinsic luminosity, but very rare within a galactic disk. The radio ELGs we observe, on the other hand, are analogous to G, K, and M type stars, far less luminous, but much more common in the local volume. In flux-limited surveys the radio-loud galaxies are being over-sampled, while the more common radio galaxies are under-represented. This is just an example of the Malmquist effect that is seen in flux-limited stellar surveys. Our result implies that we have greatly reduced the sample bias caused by the Malmquist effect and are detecting mostly “normal” radio-emitting galaxies within the KISS volume.

Further insight into the physical properties of this sample can be obtained through the direct comparison of the radio power and absolute magnitude for the KISS galaxies (Figure 13). Galaxies are plotted using different symbols based on their activity types, as indicated by the legend to the figure. Objects with high redshifts, which tend to be the most luminous objects, are circled in the plot. A weak but definite trend of increasing radio power with increasing optical luminosity is seen in the low redshift sample. Linear least-squares fits were calculated for each of the various types of ELGs within our sample (excluding the Seyfert 1s, which are too few in number to give a reliable fit). The fits we calculate for the Seyfert 2s, LINERs, and starbursts are:

$$\text{Sy2} : \log(P_{1.4GHz}) = (-0.20 \pm 0.11) \cdot M_B + (18.49 \pm 2.11) \quad (3)$$

$$\text{SB} : \log(P_{1.4GHz}) = (-0.32 \pm 0.04) \cdot M_B + (15.71 \pm 0.80) \quad (4)$$

$$\text{LINER} : \log(P_{1.4GHz}) = (-0.27 \pm 0.10) \cdot M_B + (16.77 \pm 1.93) \quad (5)$$

The galaxies appear to follow a linear relationship,

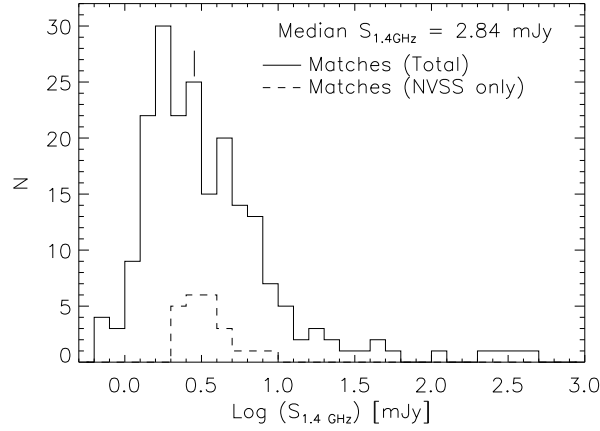


FIG. 11.— Distribution of the radio flux densities of the combined FIRST and NVSS detections for KISS ELGs.

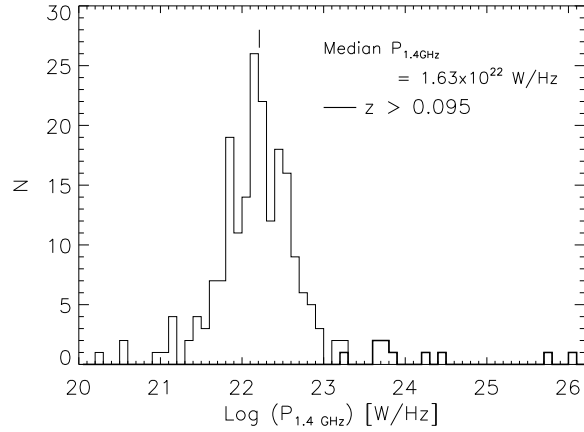


FIG. 12.— Radio power distribution for the radio ELG sample. All galaxies represented by the heavy histogram have redshifts greater than the  $\text{H}\alpha$  selection limit ( $z > 0.095$ ).

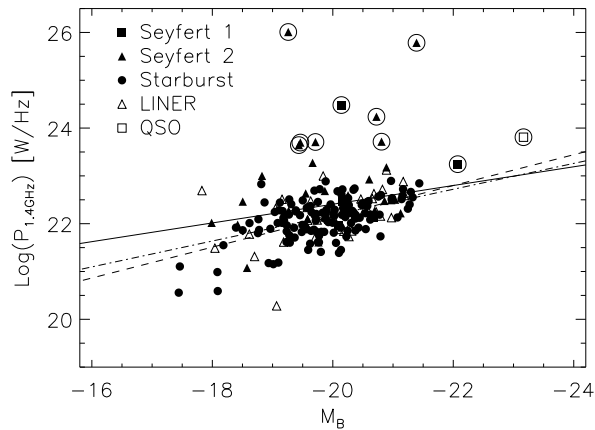


FIG. 13.— Radio power vs. optical absolute magnitude. The correlation does not appear to be very strong, however, a definite trend does exist among the ELG types. The lines are the fits to the starburst (dashed), Seyfert 2 (solid), and LINER (dashed-dotted) populations. Circled symbols represent objects detected at  $z > 0.095$  and are not included in the linear least-squares fits.

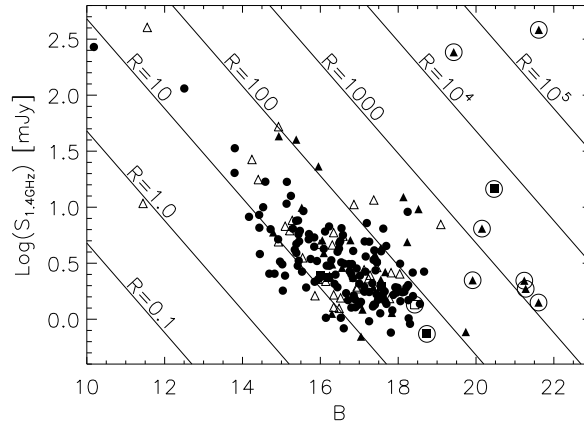


FIG. 14.— Radio flux density versus B magnitude; lines represent constant radio to optical ratio (see Eq. 6). The symbols represent the same ELG types as described in Figure 10 and include Seyfert 1s (filled squares) and one QSO (open square).

though not as tight as the well-documented radio power-FIR relationship (Condon 1992; Yun, Reddy & Condon 2001). There is also a modest trend toward more luminous galaxies in the optical being more luminous in the radio wavelengths. The fits of the starburst and LINER components of the sample are almost identical, while the Seyfert 2s tend toward slightly higher radio powers. All fits are the same within the formal uncertainties, due to the scatter of each type of galaxy about the mean relation. These fits do not include the high  $z$  Seyferts, represented by the circled symbols. A possible cause for the very similar fits between the starburst and LINER populations is that the LINERs we detect as radio sources may be driven more by star-forming activity than AGN activity. However, this is purely speculative. Moreover, given the small difference between the Seyfert 2 and LINER fits, the alternative hypothesis that the LINERs share the same activity source as the Seyferts remains plausible. It is worth noting that few surveys of this type have detected such a large LINER population. Multiwavelength observations of the current sample of KISS LINERs may be useful in unraveling the enigmatic nature of these objects.

An unexpected result from our survey is that of the comparative distribution of ELGs by type. One might initially expect AGNs to dominate at higher radio power or at higher optical luminosities and starbursts to be concentrated near the fainter end, but Figure 13 shows this is not the case. The distribution of each type of ELG appears quite similar. This means that while Seyferts typically are more luminous when compared to starburst ELGs, this is not necessarily the case in the radio wavelengths. The same is true for LINERs. Another interesting result is that at lower radio and optical luminosities, the number of galaxies dwindles, and then abruptly drops to zero. This is not due to a lack of galaxies at those optical luminosities within the KISS volume. On the contrary, there are a large number of lower luminosity and dwarf galaxies that have been classified as actively star forming, but do not appear to have detectable radio emission. This could suggest that radio emission at sufficient levels to be detected by FIRST or NVSS is only possible beyond a certain luminosity threshold. Since the 1.4 GHz emission from star-

forming galaxies is dominated by synchrotron radiation which requires a galactic-scale magnetic field, it is possible that these low-luminosity galaxies with starbursts and star-forming regions do not emit in the radio due to a lack of a sufficiently strong magnetic field. Therefore, while ELG type may not constrain the radio luminosity of a galaxy, the mass of the host galaxy may.

Another analysis tool we employ is the comparison of radio flux densities against the B magnitudes. Such a plot is shown in Figure 14 for the full KISS sample. Superimposed are lines representing constant values for the radio-to-optical ratios,  $R$ , defined by Condon (1980) as

$$R = S_{1.4} \cdot 10^{0.4(B-14.2)} \quad (6)$$

where  $B$  is the apparent magnitude. The equation is offset in the exponent from the original equation derived by Condon to better compare our  $B$  filter magnitudes to the red and near-IR filters employed by Prandoni et al. (2001) and Yun, Reddy & Condon (2001). Our results show a strong clustering of galaxies in the range of  $1.0 < S_{1.4} < 6.3$  mJy and  $10 < R < 100$ . Again, we see that the various types of ELGs overlap each other in the diagram. To be sure, the objects with  $R \geq 100$  have tendency to be AGNs (10 of 17 low redshift objects and 8 of 8 high redshift (circled) objects). However, between  $R = 10$  and 100, Seyferts, LINERs, and starbursts are coincident in the diagram, showing that despite the differences in the origin of the radio emission, the various ELG types exhibit radio emission of similar strength. Below  $R = 10$ , the majority of the objects are starbursts (16 of 22), although a few Seyferts and LINERs exist.

As previously noted, the flux limit of FIRST is not deep enough to directly explore the sub-mJy regime that Georgakakis et al. (1999), Gruppioni et al. (1999), and Prandoni et al. (2001) cover, but with the relatively high density of local radio-detected galaxies, we believe we are detecting the same population of lower radio luminosity galaxies found at these sub-mJy fluxes. For example, consider the spectroscopic follow-up data given by Gruppioni et al. (1999). They attempt to ascertain the nature of the sub-mJy population of the Marano Field from a sample of 68 faint radio sources ( $S > 0.2$  mJy). They were successful in obtaining redshifts and activity classes for 34 of

these objects. If we examine only their late-type spiral class, which equates to our starburst or star-forming class and accounts for 11 of the 34 objects, the redshift range is  $0.154 \leq z \leq 0.368$ . The flux range of these galaxies is  $0.28 \leq S_{1.4} \leq 0.60$  mJy, with one brighter galaxy at  $S_{1.4} = 1.71$  mJy. Considering that all these galaxies lie beyond the KISS redshift range, if we were to scale their distances to the median redshift of our sample, the observed flux would be well above our detection limit, and brighter than many galaxies in our sample, regardless of type. One late-type galaxy with a radio flux of  $S_{1.4} = 0.28$  mJy, an optical magnitude of  $V = 18.48$ , and a redshift of  $z = 0.255$ , is 2.4 times as far as the KISS volume limit of  $z = 0.095$ . If the object is scaled to this limiting redshift it would have an observed flux of 1.6 mJy, well within the detection range of FIRST or NVSS and easily detectable as an ELG by KISS. Thus, if this object is a typical sub-mJy detection for flux-limited surveys, we are apparently detecting the same population of galaxies.

As another example, we detect the starbursting and star-forming late-type galaxy population that dominated at the sub-mJy flux level detected by Prandoni et al. (2001) within the same  $R$  range. The majority of AGNs detected by Prandoni et al. (2001) are also within  $10 < R < 100$ , as are the majority of radio-KISS sample AGNs. When we ignore the high redshift galaxies, indicated by the circled symbols, we find that no radio-detected KISS ELG has an  $R \geq 1000$  and only a handful have  $R \geq 100$ . This is the regime that is found to be dominated by early-type galaxies, which are detected in large numbers by Prandoni et al. (2001). However, within our volume of  $z \leq 0.095$ , they detect only 2 early-type galaxies. Thus, the domination of early-type galaxies in the mJy regime may be due to the Malmquist effect, in which these luminous galaxies are detected *en masse* at higher redshift but may not be at all common in the local volume. Amplifying this effect is the observed cosmic evolution of radio galaxies, whose volume density increases with increasing redshift (Condon 1989). During the process of matching the radio catalogs with optical KISS counterparts, many strong radio sources were found within the KISS fields that were not associated with an ELG but did have optical counterparts, most of them faint objects. Either these objects possess emission lines that are fainter than the optical detection limits of KISS, they lie at redshifts beyond 0.095, or they are early-type galaxies with strong radio sources but weak or absent emission lines. Work has begun in obtaining spectra for the brighter radio objects within the KISS fields. Preliminary results indicate that many are indeed early-type and most likely elliptical galaxies, although most lie at redshifts beyond 0.095. Once these objects have all been observed spectroscopically we will be able to account for this missing population in the radio luminosity function within the KISS volume, leading to a truly complete volume-limited luminosity function (see below).

## 5. THE LOCAL RADIO LUMINOSITY FUNCTION AT 1.4GHZ

A useful way to visualize the make-up of any extragalactic sample of objects is through the construction of that sample's luminosity function (LF). The KISS ELG sample is particularly well suited for this task, since its completeness limits and selection function are both well understood

and readily quantified using the survey data. Due to the digital nature of the survey, KISS is superior in this regard when compared to previous objective-prism surveys for active galaxies carried out using photographic plates.

The calculation of the radio luminosity function (RLF) for the KISS ELGs is dependent on the careful definition of the limiting volumes of each galaxy in our sample. Each galaxy has associated with it three different selection limits which reflect the ability of both the KISS and radio surveys to detect it. They are the limiting emission-line flux level of KISS, the filter-imposed redshift limit of KISS, and the radio flux limit of either FIRST or NVSS (whichever is appropriate). The relevant volume that defines the contribution of each source to the RLF is determined by a multivariate selection function, defined by these three observational limits. Specifically, the three limiting volumes are (1) the limiting optical volume,  $V_{opt}$ , which is dependent on the completeness limit of the sample in the optical, the absolute brightness of the galaxy determined from the emission-line intensity, and the redshift of the galaxy; (2) the volume limit of KISS,  $V_{KISS}$ , which is imposed by the H $\alpha$  filter bandpass; and (3) the limiting radio volume,  $V_{rad}$ , which is set by the radio flux limit of the survey from which the flux was measured (either FIRST or NVSS) and the derived radio power of the source. The volume set by each of these limits is computed from the maximum distance that a galaxy could have and still be detected by each technique. The final volume used for each galaxy in the RLF computation is the smallest of the three volumes described above. These volumes are then used to calculate the space density within each luminosity bin of the RLF.

For most luminosity functions that are derived from a flux-limited sample, correcting for the lack of completeness in the sample is necessary in order to accurately portray the volume densities of galaxies in the sample. This is particularly true for low luminosity galaxy samples that usually suffer from incompleteness. This incompleteness is minimized in the KISS RLF, due to the nature of the survey. The majority of the radio-detected sources have  $V_{KISS}$  as their minimum volume. However, the limiting redshift set by the KISS filter is not a hard limit. As is seen in Figure 5, the number of galaxies in the survey begins to drop at  $z > 0.085$ . This is due to the fact that galaxies with weaker emission lines start to drop out of the sample as their lines redshift out of the bandpass of the objective-prism data (Salzer et al. 2000). To ensure the most complete sample possible for the calculation of the RLF, we use only objects with  $z \leq 0.085$ , which totals 184 galaxies. This eliminates the 10 high  $z$  galaxies from the sample (which we would have excluded anyway), as well as 13 galaxies with redshifts between  $z = 0.085$  and 0.095. All of these latter galaxies have radio luminosities very near the median value, meaning that we are not biasing the resulting RLF by excluding these sources. In addition, we have removed two ELGs with very small redshifts ( $z < 0.0025$ ) since their small limiting volumes cause them to make inappropriately large contributions to the computed volume densities in their respective luminosity bins. Hence, the total sample used for the RLF derivation is 182 KISS ELGs.

We adopt the cosmology of  $H_0 = 75 \text{ km s}^{-1} \text{ Mpc}^{-3}$  and  $\Omega_M = 1.0$ ,  $\Omega_\Lambda = 0$ , and  $\Omega_k = 0$  for a flat,  $\Lambda = 0$ , uni-

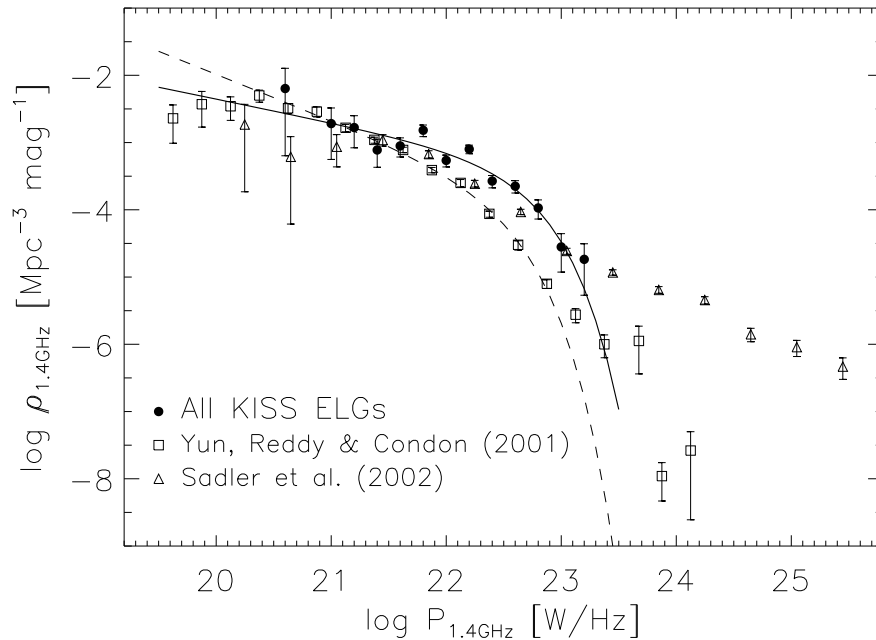


FIG. 15.— Radio luminosity function (RLF) derived for the KISS ELGs in the local volume of  $z \leq 0.085$ . The filled circles and solid line show our own data and the associated Schechter function fit. The squares and dashed line show Yun, Reddy & Condon (2001) data and associated Schechter fit for low luminosity galaxies. The triangles represent the RLF from Sadler et al. (2002).

verse throughout all our calculations. These choices allow us to directly compare our RLFs with RLFs from previous papers. The space density at each luminosity bin is calculated via the  $1/V_{max}$  method (Schmidt 1968). We compute  $V_{KISS}$ ,  $V_{opt}$ , and  $V_{rad}$  for each source and substitute the smallest of these quantities for  $V_{max}$  to obtain the final limiting volume for a particular galaxy. Using our adopted KISS redshift limit of 0.085, the limiting KISS volume ( $V_{KISS}$ ) for the luminosity function is computed to be  $2.1 \times 10^5 \text{ Mpc}^3$ . This is the maximum volume for any galaxy within our survey. The calculation of  $V_{opt}$  is based on the observed emission-line flux of each source, as measured from the objective-prism spectra. Using the line fluxes for the full KISS sample, we have derived a completeness limit for the survey, which is used to evaluate the maximum distance out to which each source can be detected based on its line strength. This distance is then used to compute  $V_{opt}$ . Full details, including the derivation of the limiting line flux of the KISS sample, is given in Gronwall et al. (2004b). The radio visibility function is calculated by solving for the distance to the galaxy in terms of the radio luminosity and calculating the radio visibility for each galaxy via

$$V_{rad} = 1.011 \times 10^{-25} \left( \frac{P_{1.4}}{S_{lim}} \right)^{3/2} \quad (7)$$

where  $V_{rad}$  has units of  $\text{Mpc}^3$ ,  $P_{1.4}$  is in units of  $\text{W/Hz}$ , and  $S_{lim}$  is the radio flux limit for the galaxy. If the galaxy is detected by both FIRST and NVSS or only by FIRST,  $S_{lim} = 1.0 \text{ mJy}$ . If detected only by NVSS,  $S_{lim} = 2.5 \text{ mJy}$ .

Once all three selection limits are taken into account, each of the 182 KISS ELGs included in the RLF calculation is assigned into one of three subsamples. The

KISS volume-limited subsample, where the volume is set by  $V_{KISS}$ , includes 98 objects (54% of the total). The radio-flux-limited subsample accounts for an additional 66 ELGs (36%). The smallest subset is the optical emission-line-flux-limited subsample, which comprises only 18 objects, or 10% of the overall sample.

Since we employ the  $1/V_{max}$  estimator for computing our luminosity functions, we are susceptible to variations in the large-scale structure (LSS) within our survey volumes. In particular, the second survey strip includes a section of the Boötes void. One might assume that the presence of this low-density region will reduce the overall amplitude of our RLF. However, we stress that the void covers less than 4% of the volume of the 2nd survey strip (Gronwall et al. 2004a), and hence less than 2% of the overall volume used for computing the current RLF. Furthermore, the depth of the KISS survey ensures that variations in the LSS are effectively averaged over since the survey samples the galaxian distribution over at least a few coherence lengths. Therefore, we do not believe that LSS variations are dramatically affecting our RLF. This belief is supported by our computation of an optical LF for the first survey strip (Gronwall et al. 2004b) using both the  $1/V_{max}$  method and the inhomogeneity-independent Lynden-Bell “C” method (Lynden-Bell 1971; de Lapparent, Geller, & Huchra 1989). The LFs computed via the two independent methods were indistinguishable in terms of their shapes, suggesting that LSS variations are not causing significant problems when only the  $1/V_{max}$  method is used.

Figure 15 shows the derived KISS RLF, plotted as filled circles. For comparison, we also plot the RLFs derived by Yun, Reddy & Condon (2001) (henceforth YRC, open squares) and Sadler et al. (2002) (henceforth S02, open

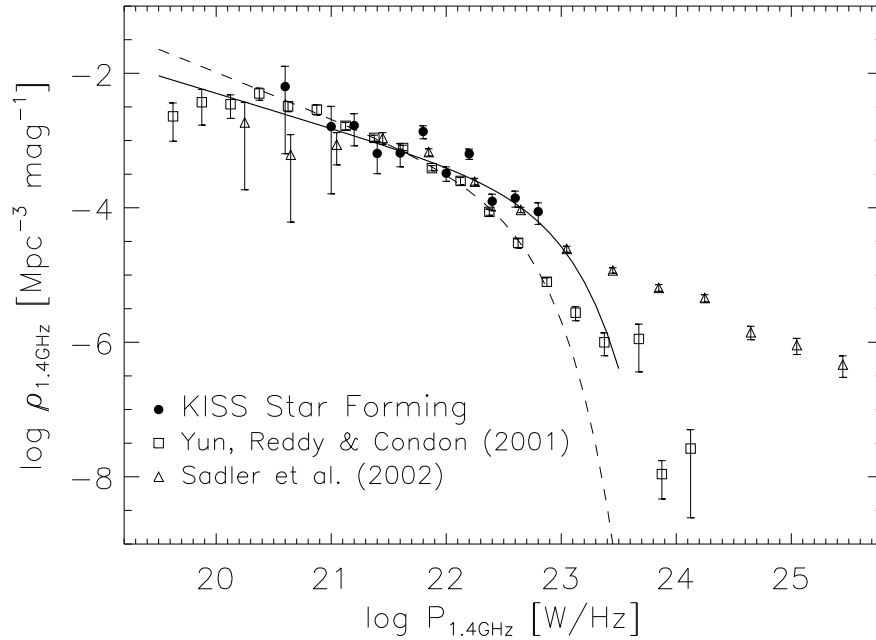


FIG. 16.— KISS RLF derived for the starburst galaxies only (filled circles). The additional RLFs and Schechter fits plotted are the same data sets as described in Figure 15.

triangles). The YRC sample is derived from a correlation of the NVSS with a catalog of IRAS-detected galaxies, and includes 1809 galaxies with redshifts as high as 0.16. Hence, it is selected via a combination of the IRAS and NVSS selection functions and flux limits. The S02 sample represents those galaxies from a subset of the 2dF redshift survey detected by NVSS, and consists of 757 galaxies with redshifts out to 0.44. The selection function for this sample is thus a combination of the NVSS and 2dF limits (see S02). The S02 RLF has been corrected to  $H_0 = 75 \text{ km s}^{-1} \text{ Mpc}^{-3}$ . The solid line in Figure 15 represents the Schechter (1976) function fit to the KISS RLF, while the dashed line is the Schechter function fit to the lower luminosity galaxies only ( $P_{1.4} < 10^{23.2} \text{ W/Hz}$ ) of YRC. The Schechter function has the form

$$\rho(L)dL = \rho^* \left(\frac{L}{L^*}\right)^{-\alpha} \exp\left(-\frac{L}{L^*}\right) d\left(\frac{L}{L^*}\right). \quad (8)$$

The parameters  $\rho^*$  and  $L^*$  are the characteristic density and luminosity of the population and  $\alpha$  describes the faint-end power-law slope for  $L \ll L^*$ . Figure 16 shows the RLF for just the KISS star-forming galaxies, along with the same RLFs from YRC and S02 for comparison. The volume densities from both KISS RLFs are listed in Table 4, along with the corresponding numbers for the AGNs (not plotted separately). The formal errors listed in the table and illustrated in the two RLF plots are based on  $\sqrt{N}$  uncertainties in each luminosity bin. Table 5 lists the Schechter parameters for the full radio sample and the starburst-only RLFs, along with the values obtained from the fit to the YRC data. We do not attempt to fit the S02 RLF, as it does not appear to be well represented by the shape of the Schechter function.

The full KISS galaxy RLF (Figure 15) agrees well with the RLF for the IRAS-NVSS sample of YRC. Below  $P_{1.4} =$

$10^{22} \text{ W/Hz}$  the two RLFs lie on top of each other. Above  $P_{1.4} = 10^{22} \text{ W/Hz}$  the KISS RLF exceeds that of YRC by a modest amount out to the last point plotted at  $P_{1.4} = 10^{23.2} \text{ W/Hz}$ . Most of the excess between the KISS and YRC RLFs above  $P_{1.4} = 10^{22} \text{ W/Hz}$  is probably due to sample differences. The IRAS-based sample of YRC is made up predominantly of star-forming galaxies ( $\sim 99\%$  according to YRC), while the KISS radio-detected sample includes a large contribution from AGNs. Fully 33% of the redshift-restricted sample of 182 galaxies used to derive the KISS RLF are AGNs. When the RLF is computed for the star-forming galaxies alone (Figure 16), the YRC and KISS RLFs agree even more closely. In both cases, the YRC RLF reaches to higher radio luminosities than does the KISS sample. This is most likely due to the fact that the KISS sample is truncated in redshift. This redshift limit greatly restricts the distance and hence the volume that KISS is probing, meaning that KISS is not sensitive to the relatively rare radio-luminous objects. As seen in Figure 12, there are in fact KISS galaxies with  $P_{1.4} > 10^{23.5} \text{ W/Hz}$ . However, these are all higher redshift objects that are not part of the quasi-volume-limited sample being used to construct the RLF. There are no radio loud galaxies within the KISS volume that have emission-line strengths high enough to be selected by KISS. The YRC sample probes roughly twice as deep in redshift and detects some rare radio luminous starburst galaxies at  $P_{1.4} > 10^{23.5} \text{ W/Hz}$ .

The similarities and differences between the KISS and YRC RLFs are echoed in the Schechter function parameters listed in Table 5. For the full KISS RLF, the Schechter fit exhibits both a shallower faint-end slope and a somewhat higher value for  $L^*$  than the YRC data. The latter is almost certainly due to the significant contribution from



the AGNs to the KISS RLF. When the AGNs are removed and only the KISS star-forming galaxies are considered, the faint-end slope  $\alpha$  more nearly agrees with the value derived from the YRC sample; they are consistent with each other within the uncertainties. Note that the value of  $L^*$  for the KISS star-forming RLF is poorly constrained by the data and must be treated with caution since the formal value for  $L^*$  is located at the highest-luminosity bin in the RLF. In general the uncertainties in all of the fitting parameters are higher for the KISS RLFs than the YRC RLF, due to the smaller number of objects present in the KISS radio sample.

The situation is different for the comparison between the KISS and S02 RLFs. The latter exhibits a shallower faint-end slope than either the KISS or YRC RLF, and lies significantly below the other two at low radio powers. However, the S02 and KISS functions agree quite well at intermediate luminosities (between  $P_{1.4} = 10^{21.4}$  W/Hz and  $P_{1.4} = 10^{23.2}$  W/Hz). Then, at radio powers above  $10^{23.2}$  W/Hz, the S02 RLF greatly exceeds both the KISS and YRC functions. The S02 sample is derived from the deep 2dF redshift survey, and includes objects out to  $z = 0.438$ . The majority of the S02 sample are AGNs, particularly those with redshifts beyond  $z = 0.15$  where  $\sim 90\%$  of their radio detections correspond to AGNs. Because of the large volumes covered by the S02 sample, they detect many more of the rare radio-loud galaxies that are largely excluded by the redshift limit of KISS. Thus, while S02 appears to be under-sampling the radio population at low powers, it is quite sensitive to the very powerful radio galaxies. The large differences between the YRC and S02 RLFs at  $P_{1.4} > 10^{23}$  W/Hz emphasizes the fact that essentially all radio-loud objects in the universe are AGNs. Note that when the S02 sample is broken down into AGNs and star-forming subsamples, the RLF for the star-forming galaxies does agree well with the KISS starburst RLF at low and intermediate luminosities (see Figure 15 of S02).

One might be concerned that the KISS sample may be missing substantial numbers of radio sources that lie within the survey volume but which have either weak or no emission lines. After all, a large number of radio-loud galaxies exhibit spectra characteristic of elliptical galaxies. However, since the KISS RLF agrees well with both the YRC and S02 RLFs in the radio power range covered by KISS, it would appear that this is not a substantial problem below  $P_{1.4} = 10^{23.2}$  W/Hz. At higher radio luminosities, the volume densities found by S02 are below  $10^{-5}$  Mpc $^{-3}$  per luminosity bin. Since the volume limit of KISS is  $\sim 2 \times 10^5$  Mpc $^3$ , the number of radio sources that might be missed by KISS is  $\sim 2$  or less in each of the luminosity bins of Figure 15 ( $\sim 5 - 6$  galaxies total). Hence, the KISS RLF is essentially undetermined for  $P_{1.4} > 10^{23.2}$  W/Hz. It would clearly be of interest to know more precisely which radio sources in the KISS volume are missed by the optical objective-prism survey, and what their properties are. For example, Miller & Owen (2002) found a large population of cluster galaxies that seem to host dust-obscured starbursts yet whose spectra are devoid of emission lines. Knowing how significant such a population of optically-obscured star-forming galaxies might be would have important implications for our understanding of galaxy evolution and the local star-formation rate den-

sity. As mentioned in the previous section, we are in the process of obtaining spectra of the optically bright galaxies with radio detections that lie in the KISS regions. To date, only two objects with radio detections have been identified within the KISS volume, consistent with the estimates above. We will continue to pursue this issue with additional spectroscopy in the future.

## 6. SUMMARY AND CONCLUSIONS

We have taken advantage of the existence of three unique wide-field surveys to carry out a multi-wavelength study of a deep sample of active galaxies. Using the optically selected emission-line galaxies from the first two H $\alpha$ -selected lists of the KISS project, we have correlated the positions of 2157 ELGs with both the FIRST and NVSS 1.4 GHz radio surveys. Among the goals of this study are to determine the incidence of detectable radio emission from star-forming galaxies and AGN, and to develop a picture of the characteristics of radio galaxies in the local universe ( $z < 0.1$ ). While most studies based on radio surveys have focused on the optical characteristics of flux-limited samples of radio sources, we instead desire to probe the radio characteristics of an optically-selected, quasi-volume-limited sample of ELGs.

Our positional matching exercise yielded a total of 207 radio detections (9.6% of the full KISS sample). Of these, 184 were detected in FIRST and 147 in NVSS. We used a variety of visual checks to evaluate the reality of all possible matches with radio-optical separations of less than 30 arcsec. Therefore, we feel that our final catalog of radio-detected KISS ELGs should be extremely reliable. The median positional difference between the FIRST and KISS galaxies is 0.75 arcsec, with only 5 matches being more than 2 arcsec apart. For the NVSS-KISS detections, the median separation is 3.4 arcsec (reflecting the lower spatial resolution of NVSS), with all but 2 of the radio sources located within 15 arcsec of the optical target.

An important aspect of our study is that all of our 207 radio-detected ELGs possess a follow-up spectrum in the KISS spectral database. These spectra provide confirmation that the KISS ELG candidates are in fact a *bona fide* emission-line source, plus yield accurate redshifts and line ratios. The latter are employed as diagnostics of the type of activity present in each galaxy.

To gain insights into the nature of the KISS radio galaxies, we first compare the optical properties of the radio-detected ELGs with the large number of radio-quiet KISS galaxies. The redshift distributions of the radio and non-radio populations are indistinguishable, indicating that the radio subsample is not biased with respect to distance. However, the radio-detected sources are on average significantly brighter (median B magnitude of 16.84 compared to 18.21) and more luminous (median B-band absolute magnitude of  $-19.89$  compared to  $-18.87$ ) than the non-radio KISS ELGs. Few radio-detected objects have B magnitudes fainter than 18.5, and all of these are higher redshift sources. The faintest object in the radio sample has  $B = 21.61$ . The radio-detected galaxies also tend to have higher H $\alpha$  luminosities but lower H $\alpha$  equivalent widths, compared to the non-radio objects.

The availability of follow-up spectra allow us to evaluate the activity type of each radio-detected KISS galaxy.

Using standard emission-line diagnostics, we determined that 132 of 207 galaxies (63.8%) are starburst/star-forming ELGs, 37 of 207 are LINERs (17.9%), 32 of 207 are Seyfert 2s (15.5%), 5 of 207 are Seyfert 1s (2.4%), and 1 object is a quasar (0.5%). In total, 75 of 207 are AGNs of some type (36.2%), which is much higher than the overall proportion of AGNs among those KISS objects with follow-up spectra (14.7%). However, the proportion of the radio sample that are AGNs is *low* when compared to radio-selected samples of objects (see below).

The star-forming galaxies in the radio subsample represent a biased population when compared to the overall population of KISS star-forming galaxies. In the line diagnostic diagram they tend to lie in the lower excitation portion of the star-forming sequence. These are galaxies with higher luminosities and higher metallicities compared to the overall KISS star-forming galaxy population. The many intermediate and lower luminosity KISS star-forming galaxies are completely absent from the radio-detected population. We interpret this as being due to, at least in part, the relative weakness of galaxian-scale magnetic fields in dwarf galaxies.

The median radio flux of the combined FIRST and NVSS radio detections is 2.84 mJy. Four sources have radio fluxes in excess of 100 mJy: KISSR 29 (= NGC 4278), which is one of the brightest objects in the KISS catalogs, and is a nearby ( $z = 0.0020$ ) elliptical galaxy with a LINER spectrum, KISSR 1307 (= NGC 4449), the well studied nearby ( $z = 0.00063$ ) Magellanic irregular galaxy, and KISSR 1304 and KISSR 1561, both high redshift Seyfert 2 galaxies ( $z = 0.3481$  and  $0.3380$ , respectively) that are also the galaxies with the highest radio powers. The median radio power for the full sample is  $P_{1.4GHz} = 1.63 \times 10^{22}$  W/Hz, with the vast majority of the KISS objects having powers in the range  $10^{21.5}$  to  $10^{22.7}$  W/Hz. Only nine KISS ELGs have radio powers in excess of  $10^{23.5}$ , and all are high redshift objects.

An interesting aspect of the properties of the KISS sample is that the ELGs of different activity types strongly overlap in terms of their radio characteristics. The starbursting ELGs have essentially the same levels of radio power and radio-optical ratios as the LINERs and Seyferts. In other words, one cannot use the radio luminosity or some other radio parameter to distinguish between the various activity types. Based on previous studies of radio-flux-selected samples, one might have expected that the AGNs would have, on average, higher radio powers. However, in our local, quasi-volume-limited sample, the starburst galaxies are contributing just as much to the total radio power as are the AGNs. Within our volume ( $z < 0.095$ ) there are no extremely powerful radio galaxies.

A radio luminosity function (RLF) was constructed for the full KISS ELG sample, as well as for the star-forming and AGN subsamples. A total of 182 objects with  $z < 0.085$  were used for the computation of the RLF, including 122 star-forming galaxies (67.0%) and 60 AGNs (33.0%). Our RLFs agree well with those computed by Yun, Reddy & Condon (2001) for a sample of IRAS galaxies also detected by NVSS, and by Sadler et al. (2002) who matched the deep 2dF redshift survey with the NVSS. The Yun, Reddy & Condon (2001) sample complements ours, in that the galaxies are selected as having FIR IRAS emis-

sion, meaning that they are typically later-type galaxies with a substantial ISM. These authors indicate that AGNs make up only a small percentage of the IRAF-NVSS sample. Therefore it is no surprise that the KISS star-forming galaxy RLF agrees extremely well with that of Yun, Reddy & Condon (2001). The Sadler et al. (2002) sample contains a large population of strong radio sources at modest redshifts, but still agrees quite well with the KISS RLF in the intermediate radio power range ( $P_{1.4GHz}$  between  $10^{21.4}$  and  $10^{23.2}$  W/Hz).

The picture that emerges from the current study about radio emission from galaxies is somewhat different from the one that is obtained by studying the objects contained in traditional flux-limited radio surveys. Since the KISS radio sample is a quasi-volume-limited sample, it should provide a very good representation of the overall population of radio-emitting galaxies in the local universe ( $z < 0.1$ ). That population is dominated by star-forming galaxies rather than AGNs. By number, roughly two thirds of the galaxies in our sample are star-forming galaxies. In terms of their integrated radio power, the star-forming galaxies contribute 59% of the total radio emission in the KISS volume. There are no high luminosity radio galaxies in this volume, which emphasizes how rare such objects are. While they are extremely common in flux-limited radio surveys (e.g., Sadler et al. (2002), Prandoni et al. (2001), Magliocchetti et al. (2002)) that probe to high redshifts, they make up much less than 1% of the volume density of all radio galaxies. Another key difference between our sample and these radio-selected samples is that the latter typically contain 60% to 80% early-type galaxies and AGN, and relatively small populations of star-forming galaxies.

It is possible that our view of the radio galaxy population in the local universe is biased substantially by the fact that KISS will not be sensitive to elliptical galaxies with weak or no emission lines. While we cannot rule this out completely, our belief is that the number of radio galaxies within the KISS volume that we are currently missing is actually quite small. First, our RLF agrees well with that of Sadler et al. (2002) in the region where the two overlap, even though their sample is not biased against early-type radio galaxies. Second, the Sadler et al. RLF for radio powers above the highest bin covered by the KISS RLF can be used to predict the number of such galaxies within the KISS volume (see previous section). We estimate that no more than 5 – 6 galaxies are missing. Finally, we point out that at least some elliptical/early-type galaxies **are** detected by KISS. For example, KISSR 29 (= NGC 4278) is one such object. The presence of many LINERs in the KISS sample also suggests that we have at least some sensitivity to early-type galaxies with weak emission-line spectra. Hence, we feel reasonably confident that, while the KISS radio galaxy sample is probably not 100% complete, it is probably missing only a modest number of radio-emitting objects with  $z < 0.095$ .

As mentioned previously, we are interested in exploring this issue further. Therefore, we have initiated a program of spectroscopy of FIRST radio galaxies with  $B < 18.5$ , in order to fill in the missing radio-emitting galaxies within the KISS volume. Since there are no radio-detected KISS ELGs within this volume with  $B > 18.5$ ,

we are confident that by obtaining these spectra that we will be able to identify all of the remaining radio galaxies within the KISS volume, and ultimately produce a truly complete, volume-limited RLF. If our assessment about missing galaxies above is correct, the resulting RLF will not look substantially different from the one shown in Figure 15.

The reader will note that we have not discussed two key issues with regard to radio emission from galaxies. First, we have not compared our radio fluxes to FIR IRAS fluxes and constructed a FIR-radio correlation. Second, we do not attempt to derive estimates of the star-formation rates of our star-forming radio galaxies. Both of these issues will be addressed in a companion paper (Gronwall *et al.* 2004c), where we consider the FIR properties of the KISS ELGs and derive star-formation rates using FIR, radio, and optical ( $H\alpha$  flux) methods.

We gratefully acknowledge financial support for the KISS project from an NSF Presidential Faculty Award to JJS (NSF-AST-9553020), as well as continued support for our ongoing follow-up spectroscopy campaign (NSF-AST-

0071114). We also thank Wesleyan University for providing additional funding for several of the observing runs during which the important follow-up spectral data were obtained. We thank the numerous KISS team members who have participated in these spectroscopic follow-up observations during the past several years, particularly Drew Phillips, Gary Wegner, Jason Melbourne, Laura Chomiuk, Kerrie McKinstry, Robin Ciardullo, and Vicki Sarajedini. Several conversations with David Helfand during the early stages of this project were extremely helpful. We are indebted to the referee for a number of suggestions that improved the final presentation of this paper. We wish to thank the support staffs of Kitt Peak National Observatory, Lick Observatory, the Hobby-Eberly Telescope, MDM Observatory, and Apache Point Observatory for their excellent assistance in obtaining both the survey data as well as the spectroscopic observations. Without their assistance this project would have been impossible. Finally, we wish to acknowledge the use of the Digitized Sky Survey, which has been produced at the Space Telescope Science Institute under U.S. Government grant NAG W-2166.

## REFERENCES

- Baldwin, J. A., Phillips, M. M., Terlevich, R. 1981, *PASP*, 93, 5  
 Becker, R. H., White, R. L., & Helfand, D. J. 1995, *ApJ*, 450, 559  
 Beckerman, E. 1999, Honors Thesis, Wesleyan University  
 Benn, C. R., Rowan-Robinson, M., McMahon, R. G., Broadhurst, T. J., and Lawrence, A. 1993, *MNRAS*, 263, 98  
 Brinkmann, W., Laurent-Muehleisen, S. A., Voges, W., Siebert, J., Becker, R. H., Brotherton, M. S., White, R. L., Gregg, M. D. 2000, *A&A*, 356, 445  
 Condon, J. J. 1980, *ApJ*, 242, 894  
 Condon, J. J. 1984, *ApJ*, 284, 44  
 Condon, J. J. 1989, *ApJ*, 338, 13  
 Condon, J. J. 1992, *ARA&A*, 30, 575  
 Condon, J. J., Cotton, W. D., Griesen, E. W., Yin, Q. F., Perley, R. A., Taylor, G. B., Broderick, J. J. 1998, *AJ*, 115, 1693  
 Condon, J. J., Cotton, W. D., & Broderick, J. J. 2002, *AJ*, 124, 675  
 de Lapparent, V., Geller, M. J., & Huchra, J. P. 1989, *ApJ*, 343, 1  
 de Theije, P. A. M. & Katgert, P. 1999, *A&A*, 341, 371  
 Faber, S. M., Tremaine, S., Ajhar, E. A., Byun, Y.-I., Dressler, A., Gebhardt, K., Grillmair, C., Kormendy, J., Lauer, T. R., & Richstone, D. 1997, *AJ*, 114, 1771  
 Geller, M. J., Kurtz, M. J., Wegner, G., Thorstensen, J. R., Fabricant, D. G., Marzke, R. O., Huchra, J. P., Schild, R. E., & Falco, E. E. 1997, *AJ*, 114, 2205  
 Georgakakis, A., Mobasher, B., Cram, L., Hopkins, A., Lidman, C., Rowan-Robinson, M. 1999, *MNRAS*, 306, 708  
 Gronwall, C., Salzer, J. J., Sarajedini, V. L., Jangren, A., Chomiuk, L. B., Moody, J. W., Frattare, L. M., & Boroson, T. A. 2004a, *AJ*, submitted  
 Gronwall, C., Salzer, J. J., Brenneman, L., Condy, E., & Santos, M. 2004b, *AJ*, in preparation  
 Gronwall, C., Salzer, J. J., Sarajedini, V. L. 2004c, *AJ*, in preparation  
 Gruppioni C., Mignoli M., Zamorani G. 1999, *MNRAS*, 304, 199  
 Ho, L. C., Ulvestad, J. S. 2001 *ApJS*, 133, 77  
 Hogg, D. W., 1999, astro-ph/9905116  
 Kellerman, K. I., & Owen, F. N. 1988, *Galactic and Extragalactic Radio Astronomy*, ed. G. I. Verschuur, and K. I. Kellermann (Berlin:Springer-Verlag)  
 Kron, R. G., Koo, D. C., Windhorst, R.A. 1985, *A&A*, 146, 38  
 Lynden-Bell, D. 1971, *MNRAS*, 155, 95  
 MacAlpine, G. M., Smith, S. B., & Lewis, D. W. 1977, *ApJS*, 34, 95  
 MacAlpine, G. M., & Williams, G. A. 1981, *ApJS*, 45, 113  
 Magliocchetti, M., Maddox, S. J., Wall, J. V., Benn, C. R., Cotter, G. 2000, *MNRAS*, 318, 1047  
 Magliocchetti, M., *et al.* 2002, *MNRAS*, 333, 100  
 Markarian, B. E. 1967, *Astrofizika*, 3, 55  
 Markarian, B. E., Lipovetskii, V. A., & Stepanian, D. A. 1981, *Astrofizika*, 17, 619 (English transl. *Astrophysics*, 17, 321)  
 Meier, D. L. 2002, *NewAR*, 46, 247  
 Melbourne, J., & Salzer, J. J. 2002, *AJ*, 123, 2302  
 Miller, N. A., & Owen, F. N. 2002, *AJ*, 124, 2453  
 Peebles, P. J. E., 1993, *Principles of Physical Cosmology*, (Princeton: Princeton University Press)  
 Pesch, P., & Sanduleak, N. 1983, *ApJS*, 51, 171  
 Prandoni, I., Gregorini, L., Parma, P., de Ruiter, H. R., Vettolani, G., Wieringa, M. H., Ekers, R. D. 2000, *A&AS*, 146, 41  
 Prandoni, I., Gregorini, L., Parma, P., de Ruiter, H. R., Vettolani, G., Wieringa, M. H., Ekers, R. D. 2001, *A&A*, 369, 787  
 Richards, E. A. 2000, *ApJ*, 533, 611  
 Sadler *et al.* 2002, *MNRAS*, 329, 227  
 Salzer, J. J. 1989, *ApJ*, 347, 152  
 Salzer, J. J., Gronwall, C., Lipovetsky, V. A., Kniazev, A., Moody, J. W., Boroson, T. A., Thuan, T. X., Izotov, Y. I., Herrero, J. L., Frattare, L. M. 2000, *AJ*, 120, 80  
 Salzer, J. J., Gronwall, C., Lipovetsky, V. A., Kniazev, A., Moody, J. W., Boroson, T. A., Thuan, T. X., Izotov, Y. I., Herrero, J. L., Frattare, L. M. 2001, *AJ*, 121, 66  
 Schechter, P. 1976, *ApJ*, 203, 297  
 Schmidt, H. R., Antonucci, R. R. J., Ulvestad, J. S., Kinney, A. L., Clarke, C. J., & Pringle, J. E. 2001, *ApJ*, 555, 663  
 Schmidt, M. 1968, *ApJ*, 151, 393  
 Smith, M. G. 1975, *ApJ*, 202, 591  
 Smith, M. G., Aguirre, C., & Zelman, M., 1976, *ApJS*, 32, 217  
 Stephenson, C. B., Pesch, P., & MacConnell, D. J. 1992, *ApJS*, 82, 471  
 Veilleux, S. & Osterbrock D. E., 1987, *ApJS*, 63, 295  
 Veilleux, S. 2003, in *Active Galactic Nuclei: from Central Engine to Host Galaxy*, eds. S. Collin, F. Combes, and I. Shlosman. A.S.P. Conference Series, Vol 290, p. 11  
 Wegner, G., *et al.* 2001, *AJ*, 122, 2893  
 White, R. L., Becker, R. H., Helfand, D. J., & Gregg, M. D. 1997, *ApJ*, 475, 479  
 Windhorst, R. A., Miley, G. K., Owen, F. N., Kron, R. G., Koo, D. C. 1985, *ApJ*, 289, 494  
 Yun, M. S., Reddy, N. A., Condon, J. J. 2001, *ApJ*, 554, 803

TABLE 1  
ORIGINAL AND REVISED FIRST FLUX VALUES

KISS ID	Orig $F_{int}$ mJy	New $F_{int}$ mJy	% Change
27	4.19	3.94	-6.0
71	26.65	27.80	+4.3
147	68.22	71.32	+4.5
392	1.43	1.73	+21.0
419	2.41	2.08	-13.7
439	2.97	2.30	-22.6
592	2.96	3.94	+33.1
1125	6.07	6.68	+10.0
1205	4.13	6.06	+46.7
1219	5.96	6.25	+4.9
1224	2.03	4.96	+144.3
1561	3.62	242.31	+6594.0
1568	29.12	33.58	+15.3
1629	9.73	12.54	+28.9
1673	4.25	3.57	-16.0
1674	3.13	2.75	-12.1
1691	4.98	5.31	+6.6
1692	4.78	4.57	-4.4
1985	16.51	20.18	+22.2

TABLE 2  
FIRST AND NVSS SOURCE MATCHES BY ELG TYPE

Survey	ELG Classification					Total
	Sy1(%)	Sy2(%)	SB(%)	LINER(%)	QSO(%)	
FIRST & NVSS	3 (2.4)	22 (17.7)	76 (61.3)	23 (18.5)	0 (0.0)	124
FIRST only	2 (3.3)	9 (15.0)	37 (61.7)	11 (18.3)	1 (1.7)	60
NVSS only	0 (0.0)	1 (4.3)	19 (82.6)	3 (13.0)	0 (0.0)	23
Totals	5 (2.4)	32 (15.5)	132 (63.8)	37 (17.9)	1 (0.5)	207
High z	2	7	0	0	1	10

TABLE 3  
OPTICAL AND RADIO PROPERTIES OF THE RADIO ELG SAMPLE

ID	RA	Dec	B	M <sub>B</sub>	L <sub>Hα</sub>	S <sub>1.4</sub>	P <sub>1.4</sub>	z	ΔR	Survey	ELG
(1)	(2)	(3)	(4)	(5)	(6)	(7)	(8)	(9)	(10)	match	Type
	hms	dms	(mag)	(mag)	erg/s	mJy	W/Hz		(mag)	(11)	(12)
9	12:18:19.3	29:15:13.3	15.98	-20.56	3.20E41	6.41	2.88E22	0.0479	0.61	B	Sv2
11	12:18:23.4	28:58:10.7	17.14	-20.36	6.56E41	4.95	5.46E22	0.0746	0.81	B	SB
27	12:19:50.6	29:36:52.3	11.46	-19.05	1.22E40	4.19	7.39E19	0.0030	3.79	B	LIN
29	12:20:06.8	29:16:50.3	11.53	-18.06	7.44E39	402.00	3.08E21	0.0020	0.40	B	LIN
33	12:21:34.4	28:49:00.4	18.24	-18.81	9.83E41	9.09	6.72E22	0.0613	0.30	B	SB
38	12:22:19.5	28:49:54.2	15.99	-21.19	5.76E41	4.67	3.89E22	0.0649	0.20	B	LIN
53	12:25:28.1	29:09:48.5	16.60	-18.93	2.06E41	0.83	1.50E21	0.0305	1.32	F	SB
63	12:27:58.8	28:49:44.4	16.52	-20.10	1.86E41	1.55	7.58E21	0.0500	0.83	B	SB
69	12:30:26.9	28:59:14.3	17.25	-19.73	3.63E41	0.96	6.80E21	0.0600	0.85	B	SB
71	12:31:22.9	29:08:10.4	14.29	-19.69	5.38E41	26.65	1.19E22	0.0152	1.32	B	LIN
74	12:32:43.0	29:42:44.4	14.68	-20.56	9.73E40	3.82	5.44E21	0.0271	9.36	N	SB
80	12:35:24.0	29:29:31.1	15.12	-18.92	6.77E40	3.09	1.42E21	0.0155	14.00	N	SB
84	12:37:17.7	28:58:39.1	16.12	-20.80	1.17E42	6.07	3.98E22	0.0578	0.56	B	SB
90	12:39:14.6	29:42:59.0	16.80	-20.13	5.84E41	1.27	8.36E21	0.0578	3.55	F	SB
102	12:41:35.1	28:50:36.4	17.37	-19.84	7.29E40	11.59	9.94E22	0.0659	0.86	B	LIN
140	12:53:05.9	29:23:43.3	16.66	-20.37	8.95E41	1.71	1.28E22	0.0617	0.05	F	SB
145	12:54:34.8	29:36:45.3	18.06	-19.18	5.27E41	1.45	1.32E22	0.0678	0.69	F	SB
147	12:54:40.7	28:56:17.9	12.50	-20.15	3.07E40	68.22	9.12E21	0.0083	6.76	B	SB
157	12:58:09.3	28:42:30.6	15.53	-19.54	3.12E41	5.73	7.06E21	0.0252	10.20	N	SB
176	13:01:25.1	28:40:07.0	14.71	-19.02	1.71E41	3.83	1.47E21	0.0292	13.40	N	SB
177	13:01:25.2	29:18:48.0	15.38	-19.55	7.79E41	40.10	4.30E22	0.0235	1.64	B	Sv2
179	13:01:43.4	29:02:40.3	14.97	-19.99	1.35E41	2.55	2.82E21	0.0239	0.32	N	SB
188	13:04:22.7	28:48:39.0	15.42	-19.77	2.11E41	3.00	4.10E21	0.0265	0.31	N	SB
198	13:06:17.3	29:03:47.3	15.23	-20.20	2.26E41	17.62	1.91E22	0.0237	0.70	B	LIN
218	13:09:16.1	29:22:02.8	15.38	-19.29	1.60E41	4.70	4.01E21	0.0210	0.10	B	LIN
222	13:09:47.5	28:54:24.6	14.17	-20.23	7.70E40	2.72	1.80E21	0.0185	0.31	B	SB
227	13:11:01.7	29:34:41.5	15.13	-19.88	3.58E41	10.74	1.26E22	0.0449	0.68	N	LIN
242	13:16:03.9	29:22:53.7	16.71	-19.23	5.29E41	1.48	4.14E21	0.0379	1.56	B	SB
254	13:18:12.3	28:45:06.8	15.99	-19.77	3.71E41	2.36	5.60E21	0.0349	3.01	N	SB
266	13:19:58.8	29:25:38.8	15.75	-19.81	4.44E41	3.45	6.76E21	0.0317	12.30	N	SB
273	13:21:50.9	29:28:50.7	15.54	-20.28	7.29E41	4.54	8.25E21	0.0246	0.25	B	LIN
285	13:25:39.9	28:53:39.6	17.45	-19.57	2.53E41	2.90	2.19E22	0.0618	0.43	B	LIN
292	13:29:04.1	28:58:21.0	17.60	-18.96	2.18E41	1.58	7.82E21	0.0502	1.24	F	SB
332	13:40:45.2	29:08:14.1	17.15	-20.58	2.07E42	2.25	8.26E21	0.0449	0.17	N	LIN
343	13:41:03.0	29:36:42.8	17.62	-19.88	1.83E42	6.44	7.70E22	0.0776	0.66	F	SB
337	13:41:35.9	29:38:11.1	17.60	-19.90	1.33E42	1.64	1.95E22	0.0773	1.51	F	SB
349	13:45:52.1	29:45:13.3	17.45	-18.62	1.82E41	3.21	1.03E22	0.0406	0.58	F	SB
361	13:49:07.4	29:25:34.9	18.27	-19.19	7.40E41	2.19	1.82E22	0.0762	1.58	F	SB
363	13:50:34.4	29:22:22.2	16.26	-19.70	1.21E41	4.18	1.22E22	0.0386	6.00	N	SB
380	13:52:19.2	29:33:00.8	17.44	-20.03	8.48E41	1.67	1.95E22	0.0768	0.36	F	SB
392	13:56:11.3	28:59:31.9	16.31	-20.66	1.34E41	1.73	1.26E22	0.0609	1.33	B	LIN
400	13:57:15.8	29:11:31.7	17.14	-19.72	1.36E41	6.27	1.68E22	0.0371	21.90	N	SB
410	13:58:54.9	29:34:35.9	16.73	-20.76	1.81E42	3.11	3.69E22	0.0773	0.25	B	SB
419	14:00:32.7	28:39:38.8	16.31	-20.64	7.67E41	2.41	1.75E22	0.0607	1.25	B	LIN
421	14:00:59.2	29:33:44.5	15.64	-19.59	1.67E41	1.92	2.83E21	0.0276	0.66	F	SB
422	14:01:04.0	29:31:31.7	17.30	-19.31	3.72E41	4.20	1.45E21	0.0265	1.11	F	SB
424	14:01:29.6	29:14:14.1	17.85	-19.23	6.17E41	0.91	7.40E21	0.0642	2.24	F	SB
428	14:02:18.7	29:44:49.0	16.54	-20.53	3.39E42	3.22	2.59E22	0.0639	1.77	B	SB
429	14:02:49.2	29:00:44.8	15.47	-20.76	1.53E42	1.45	1.70E22	0.0730	0.48	B	SB
433	14:03:43.7	29:20:44.5	16.46	-20.62	2.42E42	1.93	1.55E22	0.0638	0.29	B	SB
434	14:03:45.1	29:21:44.0	16.09	-20.97	2.51E42	3.90	3.11E22	0.0636	0.50	B	Sv2
439	14:04:12.9	29:39:28.6	16.54	-20.97	3.81E42	2.97	3.59E22	0.0780	0.64	B	Sv2
466	14:09:45.2	29:38:38.8	18.04	-19.05	1.36E41	2.54	1.08E22	0.0645	0.90	F	LIN
486	14:13:39.6	29:34:38.7	16.86	-20.38	3.97E41	1.63	1.53E22	0.0689	0.36	F	SB
497	14:15:44.5	29:02:20.8	17.55	-20.17	7.32E41	2.25	3.30E22	0.0858	0.36	F	Sv2
501	14:16:22.6	29:33:04.0	16.94	-20.00	1.55E41	1.94	1.39E22	0.0603	0.33	B	LIN
510	14:17:36.3	29:01:31.7	15.94	-19.83	1.08E42	4.44	1.44E22	0.0542	0.46	B	SB
511	14:17:46.7	29:02:41.5	16.16	-21.33	7.11E43	3.01	3.57E22	0.0773	1.38	B	SB
512	14:17:48.5	29:03:11.2	17.37	-20.14	3.73E41	3.39	4.10E22	0.0781	0.68	B	SB
526	14:21:31.9	29:10:04.3	17.45	-20.34	3.27E41	3.26	5.12E22	0.0531	0.71	F	SB
531	14:22:20.2	29:42:55.5	15.99	-20.82	8.56E41	4.88	3.72E22	0.0531	0.71	B	Sv1
546	14:25:15.8	29:40:24.7	17.54	-19.23	2.93E41	1.13	6.92E21	0.0558	1.00	F	SB
557	14:29:07.7	29:43:42.6	16.97	-19.73	1.80E41	2.35	1.35E22	0.0541	0.26	B	Sv2
577	14:49:07.4	29:49:38.0	16.67	-19.71	2.50E41	1.35	2.60E21	0.0332	0.59	F	SB
592	14:55:31.1	29:27:33.3	17.56	-19.31	4.95E41	3.94	2.50E22	0.0568	0.18	F	SB
612	15:01:34.6	28:47:14.7	17.69	-19.40	5.09E41	1.20	9.22E21	0.0624	0.80	F	SB
616	15:02:22.5	29:43:24.1	17.81	-19.57	1.50E42	0.76	7.67E21	0.0714	0.26	F	SB
618	15:02:58.8	28:48:16.8	16.33	-20.86	3.08E41	2.88	6.63E21	0.0265	0.86	B	Sv2
659	15:12:41.7	29:15:57.4	17.93	-19.39	1.02E42	1.93	1.90E22	0.0705	0.80	F	SB
707	15:22:44.9	29:46:10.2	15.09	-19.80	4.37E41	2.45	2.57E21	0.0233	0.73	B	SB
717	15:23:25.9	28:55:03.6	18.04	-19.76	1.11E42	12.31	1.87E23	0.0874	0.48	B	Sv2
730	15:25:17.8	29:05:17.8	17.94	-19.63	1.28E42	1.90	2.34E22	0.0788	0.33	B	SB
761	15:28:01.6	28:59:58.1	17.11	-20.22	1.34E42	1.95	1.93E22	0.0708	1.08	F	SB
762	15:28:10.0	29:14:36.4	18.21	-19.04	6.87E41	1.92	1.76E22	0.0681	1.15	F	SB
789	15:31:39.4	29:30:07.7	16.90	-19.31	1.19E42	1.50	3.06E22	0.0721	0.50	F	SB
833	15:38:41.2	29:27:32.8	17.04	-20.00	9.00E41	1.43	1.04E22	0.0609	0.33	B	SB
834	15:38:50.3	29:25:26.1	16.44	-20.58	1.63E42	4.00	2.86E22	0.0603	3.63	N	SB
838	15:40:11.2	29:11:38.7	21.28	-19.71	6.67E42	1.87	5.11E23	0.3517	0.39	B	Sv2
839	15:40:52.3	29:02:02.0	17.45	-20.42	3.17E41	0.77	0.93E21	0.0421	0.72	F	SB
844	15:42:27.0	29:42:02.6	18.43	-23.17	1.38E43	1.35	6.44E23	0.4566	0.30	F	QSO
872	15:50:09.8	29:11:07.3	16.58	-21.17	1.24E42	5.52	7.59E22	0.0831	0.35	B	LIN
875	15:50:03.0	29:01:27.0	18.54	-19.01	5.27E41	1.41	1.84E22	0.0774	1.51	F	SB
896	15:54:07.1	29:35:29.2	17.13	-20.47	2.47E42	2.76	3.28E22	0.0773	0.28	B	LIN
904	15:55:17.9	29:06:22.1	16.36	-21.28	1.46E42	2.07	2.53E22	0.0785	0.50	B	SB
916	15:56:08.1	28:53:10.2	17.52	-19.58	4.13E41	1.58	1.18E22	0.0616	0.41	F	SB
921	15:57:17.8	29:04:13.3	17.43	-21.93	2.34E42	1.53	2.09E22	0.0825	0.97	F	SB
937	15:58:48.7	28:56:31.9	18.50	-19.15	3.01E41	2.61	3.22E22	0.0788	1.02	F	SB
938	15:58:48.8	29:54:50.9	18.26	-19.57	3.93E41	1.48	2.15E22	0.0855	1.19	F	SB
946	16:00:06.0	29:13:33.1	17.35	-20.35	9.39E41	1.30	1.71E22	0.0813	0.22	F	SB
947	16:00:10.9	29:10:06.9	18.02	-20.59	8.63E41	2.45	7.97E22	0.0782	1.00	F	SB
961	16:04:25.4	29:24:34.9	17.40	-20.57	5.54E41	1.35	2.35E22	0.0934	1.04	B	SB
967	16:06:31.8	29:27:57.2	17.28	-20.68	6.15E41	2.47	4.24E22	0.0926	0.56	B	LIN
971	16:06:48.1	29:10:48.4	18.74	-22.07	2.67E42	0.74	1.76E23	0.3290	0.98	B	Sv1
988	16:10:43.8	29:18:42.2	16.17	-20.17	1.98E43	1.3					

TABLE 3—Continued

ID	RA	Dec	B	M <sub>B</sub>	LH $\alpha$	S <sub>1.4</sub>	P <sub>1.4</sub>	z	$\Delta R$	Survey	ELG
(1)	hms	dms	(4)	(5)	erg/s	mJy	W/Hz	(9)	"	match	Type
(1)	(2)	(3)	(4)	(5)	(6)	(7)	(8)	(9)	(10)	(11)	(12)
1424	13:04:08.2	44:08:23.8	17.40	-19.48	1.39E41	7.22	4.92E22	0.0588	0.71	B	SB
1439	13:05:50.8	43:11:38.4	16.48	-18.76	7.37E40	4.27	6.36E21	0.0277	0.79	B	SB
1441	13:06:00.4	43:46:09.0	16.86	-19.16	3.25E41	10.56	3.24E22	0.0396	0.75	B	LIN
1461	13:08:37.9	43:44:15.6	15.16	-20.66	1.87E41	52.27	1.33E23	0.0361	0.37	B	LIN
1465	13:09:00.7	43:34:12.5	17.24	-18.61	4.60E40	2.30	6.04E21	0.0367	1.09	F	LIN
1476	13:10:42.4	44:01:27.9	14.92	-20.93	1.81E40	7.62	2.00E22	0.0367	2.99	B	LIN
1477	13:11:11.2	43:43:34.3	15.58	-19.39	8.60E40	7.61	8.83E21	0.0245	0.91	B	SB
1487	13:12:59.9	43:12:15.5	15.57	-21.44	1.36E42	9.24	6.98E22	0.0619	0.26	B	SB
1494	13:13:25.8	43:32:14.2	15.95	-20.89	1.29E42	23.12	1.51E23	0.0576	0.77	B	Sv2
1498	13:13:54.2	44:10:49.6	18.15	-19.30	2.83E41	2.60	2.97E22	0.0759	0.89	F	LIN
1511	13:15:10.1	43:25:46.8	17.58	-20.16	6.94E41	1.95	2.90E22	0.0864	0.65	F	Sv1
1527	13:17:38.0	43:48:37.5	15.53	-19.75	1.25E41	2.66	4.13E21	0.0283	0.82	B	SB
1530	13:18:33.9	43:13:41.0	17.39	-20.08	2.43E42	4.12	4.77E22	0.0764	1.31	B	SB
1533	13:18:45.7	43:14:06.7	16.34	-20.31	1.55E41	1.28	7.04E21	0.0529	1.66	B	LIN
1537	13:19:01.6	43:15:00.4	16.43	-20.20	1.28E41	1.76	9.44E21	0.0523	0.67	B	SB
1541	13:19:07.3	43:08:13.1	19.91	-20.81	6.86E42	2.23	5.19E23	0.3259	1.15	F	Sv2
1554	13:22:55.0	42:54:36.1	17.52	-19.89	7.09E41	1.76	1.95E22	0.0748	0.93	F	LIN
1566	13:23:48.5	43:18:03.9	15.52	-19.73	4.17E41	9.90	1.48E22	0.0278	1.28	B	Sv2
1561	13:24:04.3	43:34:06.4	19.43	-21.39	5.00E42	242.31	6.09E25	0.3380	0.57	B	Sv2
1568	13:25:14.0	43:16:01.6	13.91	-17.35	6.05E40	33.58	1.27E21	0.0044	0.54	B	SB
1577	13:28:43.4	43:18:10.9	16.28	-20.98	5.68E41	3.36	3.58E22	0.0693	7.99	N	SB
1578	13:28:44.0	43:55:50.3	15.91	-19.37	2.57E41	3.31	5.13E21	0.0283	0.54	B	SB
1589	13:31:00.4	42:50:12.9	16.70	-18.54	4.35E40	1.03	1.54E21	0.0277	0.84	F	SB
1592	13:31:56.0	44:08:26.1	16.22	-19.46	1.30E41	6.73	1.51E22	0.0339	1.35	B	SB
1600	13:34:20.9	42:43:08.6	21.61	-19.44	4.01E42	1.41	4.41E23	0.3746	0.89	F	Sv2
1629	13:39:35.9	43:03:10.0	15.22	-18.21	5.03E40	12.54	3.53E21	0.0121	1.04	B	SB
1631	13:39:56.6	43:29:01.5	16.84	-20.19	5.52E41	4.07	3.17E22	0.0628	0.85	B	SB
1633	13:41:02.0	43:57:25.5	16.81	-19.83	4.87E41	3.11	1.69E22	0.0526	0.80	B	SB
1664	13:51:29.5	43:48:22.2	15.38	-20.29	2.75E41	7.57	1.67E22	0.0337	1.45	B	SB
1666	13:52:33.9	43:38:33.6	16.94	-19.92	6.70E41	1.87	1.25E22	0.0582	0.09	B	LIN
1673	13:54:10.2	44:12:48.7	16.09	-20.98	6.43E41	4.25	3.43E22	0.0639	1.27	B	SB
1674	13:54:11.9	44:12:29.5	16.61	-20.49	9.34E42	3.13	2.60E22	0.0648	0.99	B	SB
1683	13:59:02.4	42:54:02.8	17.48	-19.88	1.01E42	1.49	1.57E22	0.0729	0.53	F	SB
1691	14:00:57.8	42:51:20.0	16.51	-19.08	4.51E41	4.98	1.03E22	0.0327	0.69	B	SB
1692	14:00:58.8	42:50:42.7	16.49	-19.16	1.76E42	4.78	1.04E22	0.0335	0.34	B	SB
1697	14:02:26.3	43:14:24.6	18.26	-19.50	6.62E41	2.02	3.07E22	0.0873	1.53	F	SB
1743	14:13:26.3	43:47:08.3	17.26	-20.49	6.22E41	1.75	2.62E22	0.0867	0.77	F	SB
1747	14:15:06.4	43:48:12.2	17.62	-19.65	5.06E41	1.81	1.74E22	0.0697	1.12	F	SB
1751	14:16:47.7	42:51:11.6	20.15	-20.72	1.29E44	6.44	1.72E24	0.3482	0.86	B	Sv2
1764	14:22:31.0	43:42:50.7	17.69	-19.78	1.08E41	4.51	5.27E22	0.0767	0.57	B	SB
1811	14:33:47.2	43:02:43.4	17.65	-20.15	2.05E42	1.77	2.74E22	0.0882	0.23	B	SB
1835	14:39:52.2	42:44:32.5	14.72	-18.08	1.20E40	6.36	9.73E20	0.0089	4.77	N	SB
1857	14:46:25.0	43:49:56.0	15.85	-20.43	7.62E41	2.16	8.29E21	0.0443	1.58	B	SB
1869	14:50:39.4	42:44:27.2	14.53	-19.86	2.04E41	10.00	6.75E21	0.0187	0.37	N	SB
1871	14:51:46.5	43:38:40.8	14.69	-18.09	3.86E39	2.55	3.90E20	0.0089	8.14	N	SB
1891	15:02:43.3	43:16:29.0	15.86	-20.27	7.33E40	1.62	5.37E21	0.0412	1.00	F	LIN
1895	15:03:08.7	42:38:53.3	16.84	-19.36	2.11E41	2.33	8.21E21	0.0425	1.34	F	SB
1919	15:10:09.8	43:59:57.6	16.93	-20.27	1.38E42	2.84	2.45E22	0.0661	0.62	F	SB
1930	15:15:05.5	43:09:02.0	15.21	-19.18	3.38E41	6.17	4.11E21	0.0186	0.61	B	LIN
1961	15:32:18.3	43:22:30.0	17.00	-19.72	1.19E42	2.08	1.16E22	0.0533	1.84	B	SB
1971	15:34:00.8	43:40:27.8	17.26	-20.16	1.42E42	4.92	5.23E22	0.0732	0.13	B	SB
1976	15:35:04.2	43:08:25.4	17.34	-19.73	4.16E41	2.09	1.60E22	0.0623	1.11	F	SB
1980	15:36:27.0	43:31:07.8	14.53	-20.14	4.74E41	8.54	7.14E21	0.0208	0.76	B	SB
1985	15:37:13.2	43:17:53.7	13.87	-20.70	1.66E41	20.18	1.54E22	0.0199	0.95	B	SB
1994	15:39:07.7	43:51:54.9	14.82	-19.72	1.59E41	5.17	3.81E21	0.0195	0.22	F	SB
2009	15:43:24.4	44:07:17.9	15.70	-20.21	3.05E41	5.17	1.37E22	0.0369	0.84	B	SB
2035	15:48:35.3	42:41:47.1	17.40	-18.42	5.16E42	3.82	9.50E21	0.0357	0.96	B	Sv2
2073	16:01:10.9	43:11:38.4	18.52	-18.82	1.43E41	9.62	9.99E22	0.0724	0.40	B	Sv2
2081	16:02:16.7	42:55:01.4	14.96	-20.05	2.14E41	3.27	3.98E21	0.0251	10.80	N	SB
2097	16:05:51.0	44:05:40.8	21.24	-19.46	1.68E42	2.21	4.98E23	0.3210	0.86	F	Sv2
2098	16:05:58.1	44:03:20.1	16.20	-20.09	2.81E42	2.34	9.08E21	0.0446	1.93	F	Sv1
2118	16:09:55.5	43:07:45.3	16.99	-18.66	8.98E40	2.27	4.97E21	0.0328	6.23	N	LIN
2125	16:10:20.4	43:00:35.8	16.58	-18.50	1.36E41	5.64	7.29E21	0.0258	0.67	B	SB
2129	16:11:08.8	44:10:21.8	17.67	-19.27	2.84E41	2.64	1.88E22	0.0601	0.30	B	Sv2
2130	16:11:36.4	42:45:39.3	16.90	-20.45	4.85E42	1.28	1.35E22	0.0725	1.02	B	SB
2145	16:15:31.6	42:56:23.3	16.53	-21.07	2.10E42	1.03	1.35E22	0.0812	0.73	F	SB
2148	16:15:52.4	44:09:40.3	16.75	-20.01	2.71E41	2.68	1.63E22	0.0556	1.16	B	SB

TABLE 4  
THE LOCAL RADIO LUMINOSITY FUNCTION AT 1.4GHZ

$\log_{10}P_{1.4GHz}$	ALL		STARBURST		AGN	
	N	$\log\rho_{1.4GHz}$	N	$\log\rho_{1.4GHz}$	N	$\log\rho_{1.4GHz}$
20.2	1	$-2.30^{+0.30}_{-1.0}$	0	...	1	$-2.30^{+0.30}_{-1.0}$
20.4	0	...	0	...	0	...
20.6	1	$-2.20^{+0.30}_{-1.0}$	1	$-2.20^{+0.30}_{-1.0}$	0	...
20.8	0	...	0	...	0	...
21.0	2	$-2.72^{+0.23}_{-0.53}$	1	$-2.79^{+0.30}_{-1.0}$	1	$-3.52^{+0.30}_{-1.0}$
21.2	4	$-2.78^{+0.18}_{-0.30}$	4	$-2.78^{+0.18}_{-0.30}$	0	...
21.4	5	$-3.11^{+0.16}_{-0.26}$	4	$-3.19^{+0.18}_{-0.30}$	1	$-3.88^{+0.23}_{-0.53}$
21.6	10	$-3.05^{+0.12}_{-0.17}$	7	$-3.18^{+0.14}_{-0.21}$	3	$-3.62^{+0.18}_{-0.30}$
21.8	26	$-2.82^{+0.07}_{-0.09}$	21	$-2.87^{+0.09}_{-0.11}$	5	$-3.79^{+0.16}_{-0.26}$
22.0	25	$-3.26^{+0.07}_{-0.09}$	17	$-3.48^{+0.09}_{-0.12}$	8	$-3.67^{+0.13}_{-0.19}$
22.2	47	$-3.10^{+0.06}_{-0.07}$	33	$-3.20^{+0.07}_{-0.08}$	14	$-3.79^{+0.10}_{-0.14}$
22.4	23	$-3.57^{+0.08}_{-0.10}$	13	$-3.90^{+0.11}_{-0.14}$	10	$-3.84^{+0.12}_{-0.17}$
22.6	23	$-3.65^{+0.08}_{-0.10}$	14	$-3.85^{+0.10}_{-0.14}$	9	$-4.07^{+0.12}_{-0.18}$
22.8	10	$-3.97^{+0.12}_{-0.17}$	8	$-4.06^{+0.13}_{-0.19}$	2	$-4.72^{+0.23}_{-0.53}$
23.0	3	$-4.55^{+0.20}_{-0.37}$	0	...	3	$-4.55^{+0.18}_{-0.30}$
23.2	2	$-4.74^{+0.23}_{-0.53}$	0	...	2	$-4.74^{+0.23}_{-0.53}$

TABLE 5  
SCHECHTER PARAMETERS FOR THE KISS AND YRC RLFs

Fits	$L^*$ ( $10^{22}$ W/Hz)	$\alpha$	$\phi^*$ ( $10^{-3}$ Mpc $^{-3}$ mag $^{-1}$ )	$\chi^2$
KISS: All	$4.05 \pm 0.99$	$-1.35 \pm 0.18$	$1.16 \pm 0.29$	1.66
KISS: SB	$6.03 \pm 2.00$	$-1.52 \pm 0.16$	$0.39 \pm 0.11$	3.10
YRC	$2.64 \pm 0.12$	$-1.68 \pm 0.04$	$0.49 \pm 0.03$	2.79